Mechanical Properties of Heat-Treated and Hot-Dip Galvanized Rectangular Hollow Section Material

by

Zhengyuan Ma

B.Eng., University of Victoria, 2016

A Thesis Submitted in Partial Fulfillment

of the Requirements for the Degree of

MASTER OF APPLIED SCIENCE

in the Department of Civil Engineering

Supervisory Committee

Mechanical Properties of Heat-Treated and Hot-Dip Galvanized Rectangular Hollow Section Material

by

Zhengyuan Ma
B.Eng., University of Victoria, 2016

Supervisory Committee

Dr. Min Sun, Department of Civil Engineering
Supervisor

Dr. Cheng Lin, Department of Civil Engineering
Academic Unit Member

Abstract

Hot-dip galvanizing is widely used for corrosion protection of steel structures. However, there has been a plethora of recent reports on premature cracking in galvanized steel structures, which have resulted in some early decommissions or even hazardous collapses. This research focuses on cold-formed Rectangular Hollow Sections (RHS). A total of 108 tensile coupons were tested to investigate the effects of galvanizing as well as different pre-galvanizing treatments on the material properties around the cross sections of the specimens. For the first time, this thesis reports a comprehensive measurement of residual stresses in different directions at the member ends which are directly relevant to the cracking issue. The results were also compared to the residual stresses far away from the member ends, which are relevant to structural stability research. In all, the research provides a better understanding of the characteristics and structural performance of galvanized RHS to facilitate its application. The recommendations can help engineers, fabricators and galvanizers mitigate the risk of cracking in RHS during galvanizing.

Table of Contents

List of Tables

List of Figures

Acknowledgments

I would like to thank everyone who helped me with the completion of this thesis and who made this experience both memorable and enjoyable. In particular, I would like to give Professor Min Sun, my supervisor, my sincere thanks for all of his guidance and help during the past two years. Thank you for setting such a strong example of knowledge, responsibility, wisdom, and diligence in my career, and thank you for being the mentor of my research in steel structures. To the Civil Engineering laboratory staff, Dr. Armando Tura, Matt Walker, and Geoff Burton, thank you for all the incredible knowledge, experience and help during the experimental studies. I would also like to acknowledge the financial support received from the Canadian Institute of Steel Construction (CISC), the Natural Sciences and Engineering Research Council of Canada (NSERC), and the University of Victoria (UVic). I would like to acknowledge Silver City Galvanizing, McAllister Industries, Park Derochie, and Reliable Tube for their donation of materials and services. Besides, I would like to thank my colleagues and friends, especially Kamran Tayyebi, Sara Daneshvar, Prakriti Sharma, Boyu Wang, Wei Zhang, and Kaifeng Xu for their constructive suggestions, tacit encouragements and welcomed distractions. At last but most importantly, I would like to thank my family for their continuous love, support, and Chicken Soup for the Soul.

Nomenclature

Abbreviations

% Diff.	Percentage difference
AGA	American Galvanizers Association
ASTM	American Society for Testing and Materials
CE	Carbon Equivalent
CHS	Circular Hollow Section
CSA	Canadian Standards Association
DPI	Dye Penetrant Inspection
EDX	Energy Dispersive X-ray
ERW	Electric Resistance Welding
HSS	Hollow Structural Sections
IIW	International Institute of Welding
ISO	International Organization for Standardization
JIS	Japan Industrial Standard
LME	Liquid Metal Embrittlement
RHS	Rectangular Hollow Sections
SEM	Scanning Electron Microscope
Std.	Standard deviation

Variables

a	Calibration constant for isotropic stress
b	Calibration constant for shear stress
E	Young's modulus
E_{avg}	Average of Young's moduli
f_u	Measured ultimate strength
$f_{uc,avg}$	Average of ultimate strengths of tensile coupons from corners of RHS
$f_{uf,avg}$	Average of ultimate strengths of tensile coupons from flat faces of RHS
f_y	Measured yield strength
$f_{yc,avg}$	Average of yield strengths of tensile coupons from corners of RHS
$f_{yf,avg}$	Average of yield strengths of tensile coupons from flat faces of RHS
p	Parameter to calculate isotropic, or equi-biaxial stress
P	Isotropic, or equi-biaxial stress
q	Parameter to calculate 45º shear stress
Q	45º shear stress
r_i	Inside corner radius of RHS
r_o	Outside corner radius of RHS
t	Measured wall thickness; Parameter to calculate x-y shear stress
T	The x-y shear stress

β	Principal angle
ε_1	Strain reading of transverse direction on hole-drilling test
ε_2	Strain reading of 45º direction on hole-drilling test
ε_3	Strain reading of longitudinal direction on hole-drilling test
ε_{rup}	Rupture strain determined by re-joining the fractured coupon and measuring: change in gauge length / initial gauge length
$\varepsilon_{rup,avg}$	Average of rupture strain
σ_{max}	Maximum principal stress
σ_{min}	Minimum principal stress
$\sigma_{rs,long}$	Residual stress in the longitudinal direction
$\sigma_{rs,long,avg}$	Average of residual stress in the longitudinal direction
$\sigma_{rs,tran}$	Residual stress in the transverse direction
$\sigma_{rs,tran,avg}$	Average of residual stress in the transverse direction
σ_x	Cartesian stress in transverse direction
σ_y	Cartesian stress in longitudinal direction

1.0 Introduction

Corrosion protection is important for exposed steel structures. Hot-dip galvanizing is one of the most cost-effective measures for corrosion protection. Galvanized steel structures are often maintenance-free since the service life of the zinc coating usually exceeds the design life of structure [1]. The hot-dip galvanizing procedures, illustrated in Figure 1, include: (1) surface preparation (degreasing, rinsing, pickling, rinsing and fluxing); (2) dipping of steel in the molten zinc bath; and (3) inspection. The zinc bath, containing a minimum of 98% pure liquid zinc, is typically maintained at 450ºC.

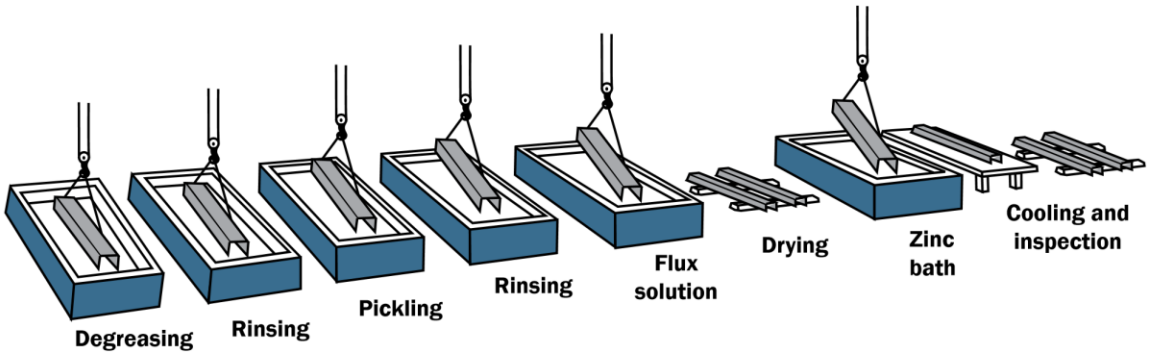

Figure 1: Hot-dip galvanizing procedures [1]

The popularity of Hollow Structural Sections (HSS) for use in construction results not only from aesthetic considerations but also from solid economic advantages [2]. In particular, the application of galvanized tubular steel structures (e.g. buildings, bridges and highways, transmission and communication towers, and industrial plants) has expanded significantly over the years. Figure 2 shows some examples of galvanized tubular steel structures composed of Rectangular Hollow Sections (RHS). The appearance, thickness, strength and durability of zinc coating depend on the chemistries of the steel and the zinc bath. This thesis focuses on only the effects of galvanizing on the mechanical behaviour of HSS material.

(a) Roof truss at T Rowe Price Parking Garage
Baltimore, MD, United States

(b) Elevated pedestrian bridge at Bob Hope Airport
Burbank, CA, United States

(c) Arthur Ray Teague Parkway Pedestrian Bridge
Bossier City, LA, United States

(d) Galvanizing of truss for Ford Pedestrian Bridge, Chicago, IL, United States

Figure 2: Examples of application of galvanized RHS structures
(Photos courtesy of the American Galvanizers Association)

The phenomena of steel cracking during galvanizing have been observed since the 1930s. They were mainly due to the high residual and thermal stresses, as well as strain aging-induced material embrittlement as a consequence of cold-forming and elevated temperature. Based on early experimental investigations using the steels available in the

1950s [3], standards have been developed for safeguarding against cracking, embrittlement, warpage, and distortion of steel components in North America [4-6]. Similar standards and guidelines have been published in other parts of the world [7-9]. These standards will be discussed in details in Chapter 2. For many years, these standards have served well. However, the embrittlement problem has resurfaced in the past decade, primarily due to: (1) the increasing application of high-strength materials and sections with large wall thicknesses, and (2) the application of new zinc bath mixtures with tin and bismuth added to enhance the quality of coating. It should be noted that the galvanizing process has been practiced with little change over a century. The new zinc bath composition has not been universally adopted while the issue of steel cracking during galvanizing has resurfaced internationally [3, 10]. For instance, premature cracking in galvanized steel structures has been reported across North America [10-15]. These cracks have caused early decommissions and even hazardous collapses which present a great threat to public safety. The Eurocodes are attempting to develop provisions to address the cracking problem as well [16], since the poor in-service performance of some galvanized steel structures has become an issue. Figure 3 shows some examples of corner cracking in RHS during galvanizing.

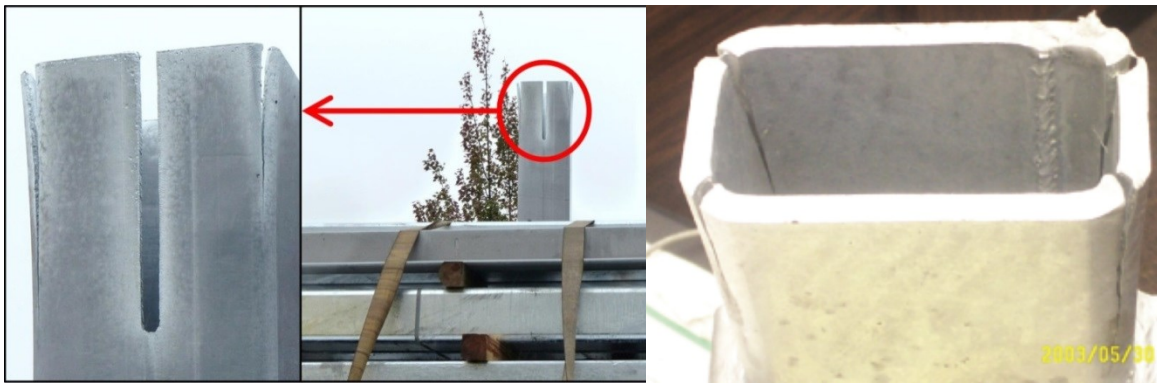

(a) Vancouver, Canada, 2016 [19] (b) Vancouver, Canada, 2003 [10]

Figure 3: Examples of cold-formed RHS corner cracking during galvanizing

On the other hand, the potential benefits of the hot-dip galvanizing process on material properties should not be neglected, other than the improvement on durability of the structures. For the purpose of supporting the sustainable development agenda, investigations have been conducted recently by Shi et al. [17, 18] from Tsinghua University in China to facilitate the application of galvanized high-strength steel in transmission towers, since they are among an electric utility's largest and most important commercial assets. The researchers found that the hot-dipping process can sometimes significantly enhance the material strength, lower the residual stress level and in turn improve the column behaviour. However, the specimens tested in the two pioneering investigations did not cover a wide range of cross-sectional shapes or dimensions.

Based on an extensive literature review [19], it was concluded that to this day, for HSS material, the relative significances of the steel-related and the galvanizing-related factors on the potential for Liquid Metal Embrittlement (LME) and accelerated strain aging had not been fully elucidated. Hence, further research on the detrimental/beneficial effects of galvanizing on the mechanical properties of HSS material is needed. In addition, new guidelines for the prevention of significant embrittlement of modern steels during

galvanizing need to be developed because: (1) the requirements in relevant standards are in general brief and qualitative; and (2) these requirements were developed based on steels available in the 1950s. In particular, experience has shown that cracking in RHS during galvanizing always initiates from the corner region at the member free end and propagates along the tube length [3, 10, 16, 20]. Hence, measurements of residual stresses in the transverse direction at the susceptible locations are needed.

2.0 Literature review

The occurrence of cracking in steel structures during hot-dip galvanizing depends on steel-related and galvanizing-related factors. These factors, including steel chemistry, material properties, residual stress, thermal stress, embrittlement mechanisms and zinc bath chemistry, are discussed in this chapter. This chapter also reviews the relevant provisions in: (1) design guides of tubular steel structures, (2) HSS manufacturing specifications, and (3) galvanizing standards.

2.1 Material-related factors

2.1.1 Steel chemistry

The appearance, thickness, strength, and durability of zinc coating depend on the chemistries of the steel and the zinc bath. The effects of certain elements in steel on the coating structures have been studied extensively and incorporated into the galvanizing standard [3]. According to ASTM A385 [4], the recommended steel chemical compositions are: $C \leq 0.25\%$, $Mn \leq 1.3\%$, $P \leq 0.04\%$, $Si \leq 0.04\ \%$ or $0.15\% \leq Si \leq 0.22\%$. Although the quality of zinc coating is also controlled by the bath temperature, immersion rate and time, the most significant factor is the steel chemistry and in particular the silicon content [3]. The well-known "Sandelin curve" (see Figure 4) shows that steel components with a silicon content less than 0.04% (Zone 1) will develop zinc coating of proper thickness on the surface during galvanizing. On the other hand, excessively thick and possibly brittle zinc coating will be developed on reactive steels with a silicon content range from 0.04% to 0.15% (Zone 2). Similarly, the coating can be excessively thick for reactive steels with a silicon content higher than 0.22% (Zone 4) [3]. A silicon content from 0.15% to 0.22% (Zone 3) is also recommended for acceptable zinc coating thickness and quality.

Recommendations based on the "Sandelin curve" have been included in the new ASTM standard for cold-formed HSS products, ASTM A1085-15 [21].

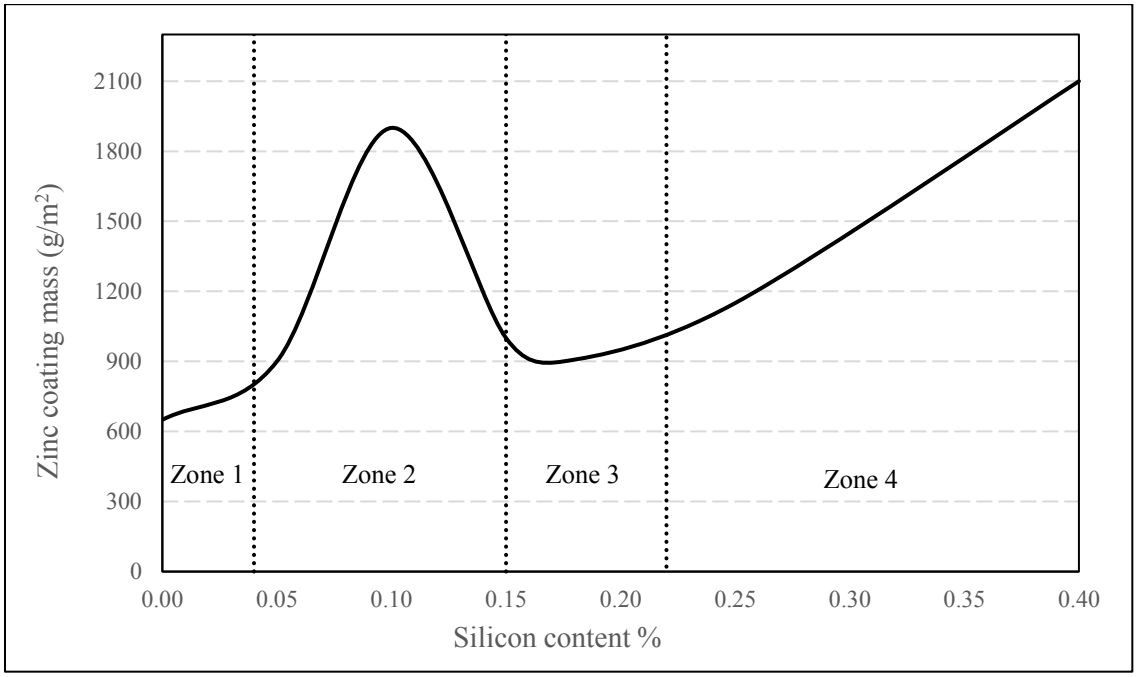

Figure 4: Effect of silicon content in steel on zinc coating thickness, 8 minutes immersion at 455ºC (adapted from [3])

The carbon equivalent (CE), which reduces the number of significant chemical compositional variables affecting the weldability of steel into a single quantity, is a useful concept for prevention of cracking during welding. The same approach has been utilized to minimize the risk of cracking in steel during galvanizing, since CE has been shown by previous investigations to have a strong link to the susceptibility of steel to LME. The International Institute of Welding (IIW) CE formula, shows here as Equation 1, was recommended by BCSA/GA [8] to control steel chemistry for prevention of cracking. The formula adopted in the Japanese standard for high-strength steel for application in transmission towers, JIS G3129 [22] is shown here as Equation 2. Equations 1 and 2 are used in Section 3.2 to calculate the CE-values of the RHS specimens. Although similar

formulas have been developed in other parts of the world, no attempt is made in this thesis to list all of them.

$$CE = C + \frac{Mn}{6} + \frac{Cr + Mo + V}{5} + \frac{Ni + Cu}{15} \leq 0.44 \quad (1)$$

$$CE = C + \frac{Si}{17} + \frac{Mn}{7.5} + \frac{Cu}{13} + \frac{Ni}{17} + \frac{Cr}{4.5} + \frac{Mo}{3} + \frac{V}{1.5} + \frac{Nb}{2} + \frac{Ti}{4.5} + (420)(B) \leq 0.44 \quad (2)$$

2.1.2 Material properties

Corner cracking during galvanizing can be avoided by using hot-finished RHS since these products have inherently better grain structure and mechanical properties as well as a low level of residual stress in comparison with their cold-formed counterparts. This is consistent with the findings of previous experimental investigations [3, 10, 20] which suggest that galvanizing-related factors have an effect on steel cracking, but only on already-susceptible material.

Hot-finished HSS are primarily manufactured in the U.K., German, France and Brazil to EN 10210 [23, 24], and the most common grade is S355J2H. This approach typically commences with a Circular Hollow Section (CHS) produced by cold-forming using the Electric Resistance Welding (ERW) approach. The circular shape is then heated to achieve full normalizing, to above the upper critical transformation temperature of 870 ºC to 930 ºC, and is formed to the desired shape in this condition. Good toughness and ductility can be achieved around the entire cross-section of the final product. Hence, RHS with small outside corner radii can be produced using this approach without having cracking problems. Note that CHS to this specification, with very large wall thicknesses and low diameter-to-thickness ratios, as used in bridges, are likely to be manufactured by the

seamless hot-forming approach [10]. However, this approach produces CHS only. ASTM A501 [25] is the American specification for hot-finished HSS. It should be noted that this specification is only to facilitate the importation of hot-finished HSS from Europe since these products are not manufactured in North America. However, hot-finished HSS is either unavailable in much of the world or prohibitively expensive. Hence, HSS is far more commonly produced by cold-forming.

2.1.2.1 Cold-forming methods

In general, heavily cold-formed steels are susceptible to LME and strain ageing [8, 10, 16]. The two mechanisms may cause significant transient and permanent losses of material ductility during and after galvanizing. The details of the two mechanisms will be discussed in Section 2.2.2.

It is well know that cold forming causes strain hardening of the steel material, hence its yield and ultimate strengths increase while its ductility decreases. With cold-formed RHS, the tightness of corner radii is critical when there is concern for RHS corner cracking during galvanizing [3]. Internationally, there are two common manufacturing methods for cold-formed RHS: direct-forming and continuous-forming. For both methods, the coil strip is progressively cold-bent into the desired shape by passage through a serious of pressure rollers, during which the rollers introduce a controlled amount of cold bending (depending on the sizes of the used rollers) to the coil strip, thus the mechanical properties are theoretically consistent in the longitudinal direction of the RHS product. However, some gradual variation in the longitudinal direction will occur – for both production methods – in practice due to the location of the final RHS member relative to the position in the hot-rolled coil material from which it was made.

The direct-forming process is illustrated in Figure 5(a) and includes: (1) roll-forming a coil strip directly into an open section with the desired rectangular shape; and (2) joining the edges of the open section by welding to form a closed rectangular shape. The continuous-forming process is illustrated in Figure 5(b) and includes: (1) roll-forming a coil strip first into a circular open tube; (2) joining the edges of the open tube by welding to form a closed circular shape; and (3) flattening the circular tube walls to form the desired rectangular shape. In North America, Europe, Japan and Australia the continuous-forming process is used almost exclusively (one exception being Bull Moose Tube in the U.S. which uses the direct-forming method). In China, the direct-forming technique has become the dominant manufacturing method for production of large-sized RHS. Mass production by this method started from 2005 and the RHS have been successfully used in the construction of Olympic stadiums, railway stations, power plants and bridges [26].

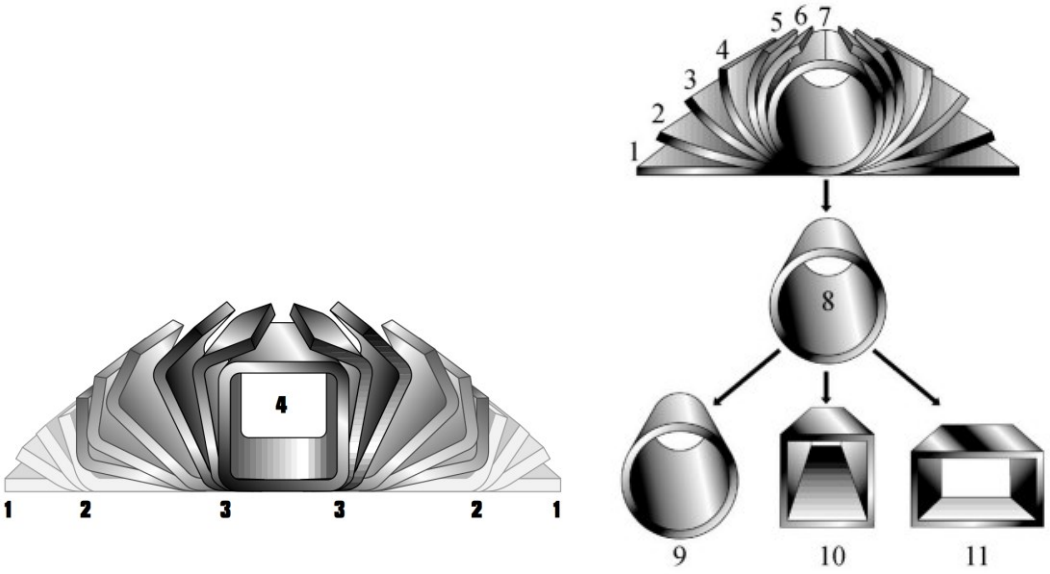

(a) Direct-forming (b) Continuous-forming

Figure 5: Cold-forming methods [19]

Although the appearance of the sections can be similar, the overall mechanical behaviours of RHS produced by different cold-forming methods can be substantially different. Extensive investigations have been conducted to capture the strength and ductility gradients around the cross-section of RHS produced by different cold-forming methods [27-32]. For direct-formed RHS, the cold-working is concentrated at the four corners, thus the flat faces (not containing the weld) of the final RHS product have similar properties to the coil material. For continuous-formed RHS, the entire cross-section contains high degrees of cold-working, thus the final RHS product has higher yield and ultimate strengths and lower ductility compared to the coil material. However, if the same coil material is used, the mechanical properties of the corner regions of the direct- and continuous-formed RHS should be similar since the coil plates are bent to similar radii [16, 33]. This deduction is consistent with the experimental evidences via tensile coupon tests [31] and Charpy V-notch impact tests [32]. Hence, for prevention of corner cracking during galvanizing, the key factor is the bending radius.

2.1.2.2 Relevant provisions in design guides for tubular steel structures

For prevention of cracking during welding, the ISO standard for welded hollow section connections under static loading [34] specifies minimum outside corner radii for welding in the zones of cold-forming without heat treatment. As can be seen in Table 1, RHS manufacturing standards often permit much lower outside corner radii. Packer et al. [10] suggest that the ISO [34] corner radius recommendations may apply equally to galvanizing as both represent criteria affected by the extreme corner residual stresses induced by cold-forming. The Chinese technical specification for structures with steel hollow sections [35] also requires that special attention be paid to the corner properties of cold-formed RHS, especially when the structure is subject to seismic or fatigue loading. This specification

suggests that when designing structures using cold-formed circular shapes, with wall thickness larger than 25 mm and diameter-to-wall thickness ratio smaller than 20, experimental investigations should be performed to study the cold-forming process, the mechanical properties of the section, the connection capacity as well as the risk of lamellar tearing. However, information on prevention of corner cracking in cold-formed RHS is limited in the Chinese specification.

Table 1: Manufacturing requirements for outside corner radii of cold-formed RHS

Specification	RHS thickness, t (mm)	Outside corner radius, r_o	
		for fully Al-killed steel (Al≥0.02%)	for fully Al-killed steel and C≤0.18%, P≤0.02% and S≤0.012%
ISO 14346:2013(1)	2.5≤t≤6	≥2.0t	≥1.6t
	6<t≤10	≥2.5t	≥2.0t
	10<t≤12	≥3.0t	≥2.4t (up to t = 12.5)
	12<t≤24	≥4.0t	–
EN 10219-2	t≤6	1.6t to 2.4t	
	6<t≤10	2.0t to 3.0t	
	t>10	2.4t to 3.0t	
ASTM A500	All t	≤3.0t	
ASTM A1085	t≤10.2	1.6t to 3.0t	
	t>10.2	1.8t to 3.0t	
CSA-G40.20/G40.21	t≤3	≤6 mm	
	3<t≤4	≤8 mm	
	4<t≤5	≤15 mm	
	5<t≤6	≤18 mm	
	6<t≤8	≤21 to 24 mm	
	8<t≤10	≤27 to 30 mm	
	10<t≤13	≤36 to 39 mm	
	t>13	≤3.0t	
AS/NZS 1163	All t, up to 50×50 mm	1.5t to 3.0t	
	All t, larger than 50×50 mm	1.8t to 3.0t	
JIS G3466	All t	≤3.0t	
GB/T 6728 for F_y > 320 MPa	t≤3	1.5t to 2.5t	
	3<t≤6	2.0t to 3.0t	
	6<t≤10	2.0t to 3.5t	
	t>10	2.5t to 4.0t	

(1) Requirements for welding in the corner regions of RHS without pre-treatment.

2.1.2.3 Relevant provisions in HSS manufacturing specifications

HSS manufacturers are aware of this issue of potential cracking, but there is no definitive published guidance on this topic from structural steel associations [10]. The suitability of cold-formed RHS for galvanizing is generally avoided in HSS manufacturing specifications, or blanket statements are given such as in EN 10219-1 ...'the products shall be suitable for hot dip galvanizing' [36]. The Australasian [37] standard discusses suitability for hot-dip galvanizing, if galvanizing is required by the purchaser, and AS/NZS even goes as far as recommending that a sample be hot-dip galvanized to determine its actual performance for a given bath and tube characteristics. The problem with such a purchaser-driven approach is that most HSS produced internationally is sold to stock-holders, so the end user or fabricator does not usually interact with the manufacturer at the time of production [10].

In general, RHS with high yield-to-tensile strength ratios are susceptible to corner cracking. The minimum specified mechanical properties for cold-formed RHS of common grades are summarized in Table 2. It should be noted that the requirements are based on tensile test specimens machined from the flat face of the RHS in the longitudinal direction [38]. Hence, they are not directly relevant for assessment of susceptibility to LME and strain ageing. The yield-to-tensile stress ratios in Table 2 are calculated using the specified minimum values. However, in reality it is very difficult for manufacturers to achieve a yield-to-tensile stress ratio smaller than 0.85, even when such measurements are taken from the middle of a flat face where the degree of cold-forming is in general the lowest around the entire cross-section [10]. The yield-to-tensile stress ratio of the RHS corner material is in general higher than that of the material in the flat face [e.g. 27-29, 31].

Table 2: Minimum specified mechanical properties for cold-formed RHS of common grades

Specification	Grade	f_y (MPa)	f_u (MPa)	f_y / f_u
EN 10219-1	S355J2H	355 for t≤16 345 for 16<t≤40	510 for t<3 470 for 3≤t≤40	0.755 for 3≤t≤40
ASTM A500	B	315	400	0.788
	C	345	425	0.812
ASTM A1085	A	345	450	0.767
CSA-G40.20/G40.21	350W	350	450	0.778
AS/NZS 1163	C350L0	350	430	0.814
	C450L0	450	500	0.900
JIS G3466	STKR490	325	490	0.663
GB/T 6725	Q345	345	470	0.734

2.1.2.4 Relevant provisions in galvanizing standards

The occurrence of instant cracking in the corner region during galvanizing depends on the interaction of residual stress, thermal stress and the transient loss of ductility due to LME. The elevated temperature during galvanizing could potentially accelerate strain ageing and cause premature deterioration of the tubular member. However, the level of permanent loss of ductility depends on the pre-galvanizing degree of cold-forming [3].

To minimize the risk of LME and strain ageing embrittlement, the ISO galvanizing standard, ISO 14713-2 [9], suggests that local cold-forming should be kept as low as possible. Where the condition cannot be fulfilled, a pre-galvanizing stress-relieving by heat-treatment is recommended. However, the standard does not specify the heat-treatment temperature or duration. Similarly, the Australasian [7] and the Chinese [39] galvanizing standards as well as the British guide for management of LME-induced cracking [8] acknowledge that the elevated temperature during galvanizing can accelerate the onset of strain ageing embrittlement of cold-formed steel, and recommend stress-relieving to suppress this phenomenon, without specifying the temperature or duration for heat-

treatment. However, experience in Canada [10] has shown that corner cracking can still occur with CAN/CSA-G40.20/G40.21 Class H RHS [40], which is stress-relieved to 450ºC. In all, it is challenging to apply the provisions in the above galvanizing standard and guidelines since they are in general brief and qualitative.

The North American standard safeguarding against galvanizing-induced embrittlement, ASTM A143 [5], advises a minimum cold-bending radius of three times the plate thickness. Although ASTM A143 does not specify whether the limit is for the inside or outside radius of the cold-bent region, it has usually been interpreted as the inside radius [3]. For steel sections with smaller bending radii, different degrees of pre-galvanizing heat-treatment are recommended. However, it is difficult to apply the provisions in ASTM A143 to modern cold-formed RHS since:

(1) The minimum cold-bending radius recommended by ASTM A143 conflicts with the corner radius requirements in certain production standards for structural steel tubing in North America. For example, ASTM A500 [8] requires that for RHS the outside corner radius shall not exceed 3t (i.e. three times the wall thickness t), corresponding to a maximum inside corner radius of 2t. The Canadian standard has similar requirements.

(2) The requirements in ASTM A143 were developed based on early research in the 1950s (reported by [3]) on the steels available at the time. Hence, the applicability to modern steel is unknown.

(3) Although ASTM A143 suggests heat-treatment of severely cold-formed steels for prevention of significant embrittlement and cracking, there is no definitive guideline on the thresholds of wall thickness above which different levels of heat-treatments are needed for tubular products.

2.1.3 Residual stress

Also associated with cold-forming is the generation of residual stress. For the purpose of compression member design, residual stress in the longitudinal direction is much more influential than that in the transverse direction. The effect of longitudinal residual stress on the compression behaviour of a steel member is to cause premature yielding, leading to a loss of stiffness and a reduction in load-carrying capacity. In previous investigations on the compression behaviour of cold-formed RHS [27-30, 41], measurements of residual stresses have been conducted using the following methods: (a) destructive approach such as the sectioning method; (b) semi-destructive approach such as the hole-drilling method; (c) non-destructive approach such as the X-ray diffraction method.

The measured longitudinal residual stresses are commonly considered as two components. The first is the membrane component (tensile or compressive depending on the measuring location), which is the mean value of the measured longitudinal residual stress which occurs uniformly through the wall thickness. The second is the bending component, which is the deviation from the mean value. Due to the existence of the longitudinal residual stress, steel samples cut from the tube walls may exhibit both axial deformation and curvature, corresponding to membrane and bending residual stresses respectively. It can be concluded from the above investigations that the compression behaviour of cold-formed RHS is mostly affected by the bending residual stress, while the membrane residual stress plays a minimal role. The residual stress levels at the corner regions of direct- and continuous-formed RHS are similar since the corner radii are similar [30, 31]. However, it should be noted that although extensive investigations on residual stresses in hollow structural sections have been conducted in the past, most of these investigations measured residual stresses in the longitudinal direction at the mid-length of

the members since they are relevant to column behaviour. Investigation on residual stresses in the transverse direction of hollow structural sections is limited. Previous research [3, 10, 16, 20], unpublished documents from Nippon Steel and Teck Cominco, as well as experience from galvanizers, has showed that cracking during galvanizing always starts at the inside surface of the corner region at the free end and propagates outwards through the tube wall and eventually down the tube length (i.e. in the longitudinal direction). Hence, measurements of residual stresses in the transverse direction at the free ends of cold-formed RHS are needed, and particularly in the corner regions.

2.2 Effects of galvanizing

2.2.1 Thermal stress

When dipped in a molten zinc bath, compressive thermal stress is first developed on the surface of the steel section since the inner colder mass acts as a restraint on the expansion of the surface material. The differential expansion stress is reduced once the inner material starts to expand. The thermal stress on the surface becomes tensile when the steel section is withdrawn from the molten zinc bath since the surface material begins to cool while the contraction is restrained by the hotter inner material. Since tensile stress is necessary for the occurrence of cracking, steel sections are more susceptible to cracking when being withdrawn from the molten zinc bath [3, 16, 20]. Previous investigations [3, 10] have suggested that cracking is triggered once the accumulative surface stress or strain (i.e. residual plus thermal) perpendicular to the direction of cracking reaches a critical value.

The thermal stresses developed on the surface of steel sections during galvanizing have been studied by researchers via site measurements and finite element simulations [3, 16, 42, 43]. It can be concluded that for typical galvanizing practices and commonly used steel

sections, the maximum tensile thermal stress generated on the material surface can be up to 400 MPa, predominantly depending on the dipping and withdrawing speeds. Hence, severely cold-formed steels could be highly susceptible to cracking since they sometimes contain high levels of residual stress. In general, the induced thermal stress decreases as the dipping and withdrawing speeds increase. For example, Kikuchi and Iezawa [42] studied experimentally and numerically the thermal stresses at the weld toe of steel plate-to-pipe joints during galvanizing. It was found that the maximum thermal stress decreases as the dipping speed or the pipe diameter increases. Similar observation was made by Kominami et al. [43] in their study on thermal stress in steel pipes during galvanizing. However, it should be noted that it is not practical to change these speeds significantly for reactivity and drainage-control purposes.

2.2.2 Embrittlement and cracking mechanisms

Other than the thermal shock, steel materials may experience a transient or a permanent loss of ductility as a result of galvanizing. Depending on the characteristics and history of the steel, numerous types of embrittlement mechanisms may occur [3, 8, 16, 44, 45]. This section discusses only the two embrittlement mechanisms relevant to structural steels of common grades: (1) liquid metal embrittlement, and (2) strain ageing. No attempt is made to discuss the other mechanisms in details. For example, hydrogen embrittlement is a potential problem for high-strength steels with tensile strength greater than 1100 MPa, since the atomic hydrogen absorbed by high-strength steels during the pickling process can significantly reduce the ductility of the material. Identification of hydrogen trapping sites in metals and their participation in brittle fracture is an ongoing field of research. A literature review on this topic can be found in [45]. Quite often the heat of the galvanizing

bath expels the atomic hydrogen absorbed by the steel during the pickling process. However, if the steel hardness is excessive, hydrogen can be retained and result in embrittlement [3, 5, 45]. Hence, when galvanizing high-strength steels and hydrogen embrittlement is of concern, pickling can be substituted by abrasive blast cleaning since the latter does not generate hydrogen [5]. Since structural steels of common grades are not susceptible to hydrogen embrittlement [3, 8, 44, 45], it is not further discussed in the following sections.

2.2.2.1 Liquid metal embrittlement

One mechanism that may cause a transient loss of ductility in structural steel of common grades during hot-dip galvanizing is Liquid Metal Embrittlement (LME). LME occurs when steel is exposed to certain low-melting point liquid metals, such as zinc, while under tensile stress. Most descriptions of the LME phenomenon suggest that the occurrence requires an accumulative surface stress (i.e. residual stress plus thermal stress) beyond the elastic limit, at which point zinc penetration through grain boundary may occur. The material ductility decreases once intergranular decohesion takes place [3, 8, 44, 45].

Motivated by reports on cracking of steel structures during galvanizing in Japan, Kikuchi and Iezawa [42] performed tensile coupon tests on steels of two different grades (SM50A and STK55). The tensile coupons were ruptured under different conditions: (a) at room temperature before galvanizing; (b) at the galvanizing temperature of 460ºC but in the absence of liquid zinc; (c) immersed in molten zinc bath maintained at 460ºC, and (d) at room temperature after galvanizing.

It was found that: (1) The hot-dip galvanizing process has only a small effect on the initial portion of the stress-strain curve; (2) The specimens immersed in molten zinc bath fractured much earlier than those under the other three conditions. The SM50A and STK55

specimens under Condition (c) fractured at 8.5% and 7.7% strains, respectively; (3) The stress-strain curves of specimens under Conditions (a) and (d) almost overlapped; and (4) The stress-strain curve from Condition (b) is below that of the base Condition (a), but the elongation before fracture remains more or less the same.

Similar observations were made in the experiments conducted by Kinstler [3]. Tensile tests were performed on steel coupons made from ASTM A36 steel (with a nominal yield strength of 250 MPa) at the galvanizing temperature of 450ºC in the presence and absence of a molten zinc bath. It was found that the elastic portion of the stress-strain curve and the yield stress were not affected by the presence of zinc. However, the coupons immersed in the molten zinc bath fractured at a 5% strain, which is even earlier than that of Condition (c) in Kikuchi and Iezawa [42].

The results of the above investigations were consistent with the aforementioned general theory of LME. However, it should be noted that the steels tested by Kikuchi and Iezawa [42] were not heavily deformed before galvanizing. The ASTM A36 steel tested by Kinstler [3] had relatively low yield strength and good ductility as well. It can be expected that for severely cold-formed steel, such as the corner region of thick-walled cold-formed RHS, the material may brittle fracture at an earlier stage during galvanizing as a result of LME, high residual stresses, relatively low ductility and possible pre-galvanizing defects.

2.2.2.2 Strain aging

Strain ageing is a mechanism that may cause a permanent loss of ductility of steel. It is associated with time-dependent diffusion of carbon and nitrogen atoms in the material. Carbon steel deformed to a critical degree may be embrittled significantly as a result of strain ageing. The resulting brittleness varies with the ageing temperature and time. At room temperature, the ageing process requires several months to obtain the maximum

embrittlement [3, 8, 44, 45]. However, the time for maximum embrittlement decreases significantly at elevated temperatures. For example, a high degree of strain ageing-induced embrittlement may occur in cold-formed steel when in contact with the 450ºC molten zinc bath. To account for the possible occurrence of the in-service ageing, the Australasian standard for cold-formed hollow structural sections AS/NZS 1163 [37] requires artificial 'strain ageing' of the test pieces prior to tensile or impact testing, so that any change in HSS properties with time is likely captured by "strain ageing" the test samples. The ageing is achieved by heating to a temperature between 150 and 200ºC for not less than 15 min, which raises the yield stress and decreases the ductility.

2.2.3 Zinc bath chemistry

As discussed in Section 2.1, the quality of zinc coating depends on the chemistries of the steel and the bath mixture. The galvanizing bath typically contains 98% zinc and 2% additives [1, 7]. Lead and aluminum have been traditionally added to the zinc bath to: (1) enhance the brightness of the galvanized coating; (2) suppress the over-reaction between zinc and steel with high silicon content to maintain a thin and ductile coating; and (3) enhance the drainage of molten zinc from the surface of the steel, and in turn to control the thickness and uniformity of the coating [3, 46-49]. However, there has been ongoing pressure to remove lead from the zinc bath for environmental and health concerns [46].

Research has been conducted by dominant suppliers, such as Teck Cominco in Canada and Umicore in Belgium, on different bath additives and their impact on zinc coating quality [3, 46]. It was found that Tin and Bismuth behave much like lead and aluminum in a zinc bath. They are effective in improving drainage, retarding the over-reaction between steel and zinc and enhancing the brightness of the coating, without the potential

environmental impacts. As a result, new zinc bath mixtures with tin and bismuth have been developed (e.g. BritePlus™ by Teck Cominco and Galveco™ by Umicore).

However, the occurrence of steel cracking during hot-dip galvanizing seems to have become more prevalent since tin and bismuth were added to the zinc bath mixture [10, 16]. According to the 2008 Nyrstar annual report [50], "between June 2000 and March 2007, Umicore produced and supplied (approximately) 45Kt of Galveco to galvanizers in various countries (corresponding to approx. 3.5Mt of steel that has been galvanized with Galveco). Umicore withdrew Galveco from the market in March 2007 as a precautionary measure following the discovery of cracking in steel that had been hot dip galvanized. It is alleged that a cause of this cracking is the use of Galveco." Similarly, in North America Teck Cominco was also blamed for its new product because the incidences of hot-dip cracking increased after the introduction of BritePlus™ [10].

Hence, Teck Cominco duly undertook some experimental research [20] into the galvanizing of contemporary RHS. It was found that the size of cracks became greater when the content of tin or bismuth exceeded approximately 0.2%. However, Teck Cominco concluded that the predominant factor affecting cracking upon galvanizing was the RHS itself, and that the zinc bath chemistry had only a small effect. Other details of this research will be discussed in Section 4. Criteria in an interim guidance document in Germany also include controls on tin and bismuth: $Sn + Pb \leq 1.3\%$ and $Bi \leq 0.1\%$ [8]. However, the document points out that "this is not an absolute limit below which either LME can be guaranteed not to occur or above which LME will definitely occur on a more then rare basis". Recently, as part of a research program for the evolution of Eurocode 3, Feldmann et al. [16] established different maximum plastic strain capacities for steel components

based on the tin content in the zinc baths. However, it should be noted that the galvanizing process has been practiced for a century, with little change in practice. The new zinc bath composition has not been universally adopted while the issue of steel cracking during galvanizing has resurfaced internationally [3]. Hence, further research in this field is needed since, to this day, the relative significances of the steel-related and the galvanizing-related factors on the potential for LME and strain ageing have not been fully elucidated.

3.0 Experimental Program

3.1 Selection of RHS material

The RHS materials examined in this study are listed in Table 3. Three 12-metre long parent tubes were produced to Grade 350W Class C according to CSA G40.20/G40.21 [40]. The parent tubes have different width-to-wall thickness ratios corresponding to different overall amounts of cold working. The materials were then cut into short lengths and subject to different pre-galvanizing treatments, which will be discussed in Section 3.4.

Table 3: Steel chemistry and calculation of carbon equivalent-values

	Chemical elements (%)												
Parent RHS	C	Si	Mn	Cu	Ni	Cr	Mo	V	Nb	Ti	B	CE per Eq. 1	CE per Eq. 2[(2)]
RHS 102×102×6.4	0.14	0.24	0.87	0.01	0.05	0.003	0.00	0.003	N/A	N/A	N/A	0.29	0.28
RHS 102×102×7.9	0.14	0.23	0.86	0.01	0.05	0.04	0.00	0.013	N/A	N/A	N/A	0.30	0.29
RHS 102×102×13	0.2	0.023	0.75	0.02	0.008	0.026	0.002	0.002	N/A	0.002	0.0[(1)]	0.33	0.31

(1) The mill test report does not include enough numbers of significant figures for Boron (B). See Chapter 2 for discussion.

(2) For chemical elements not included in the mill test reports, a value of zero is used in the calculation of the Carbon Equivalent (CE) in Eq. 2.

3.2 Determination of steel chemistry

Susceptibility to embrittlement depends almost entirely on steel composition rather than zinc bath composition [11]. This section discusses only the alloys attributed to embrittlement of steels (i.e. the chemical elements in Equations 1 and 2). The relevant elements are extracted from the mill test reports and listed in Table 3 for calculation of carbon equivalent. To confirm the accuracy of the mill test reports, compositional analysis was also carried out via Energy Dispersive X-ray (EDX) Spectroscopy using a microscopy facility (see Figure 6). For each of the three parent tubes, a thin work piece was machined. To minimize the contamination of the sample surface, the work pieces were immersed into high purity organic solvent and completely dried before entering the vacuum chamber for

analysis. For each work piece, analyses were conducted at four different locations. For each chemical element, the averages of the obtained weight percentages are calculated. A typical EDX analysis sample is shown in Figure 7.

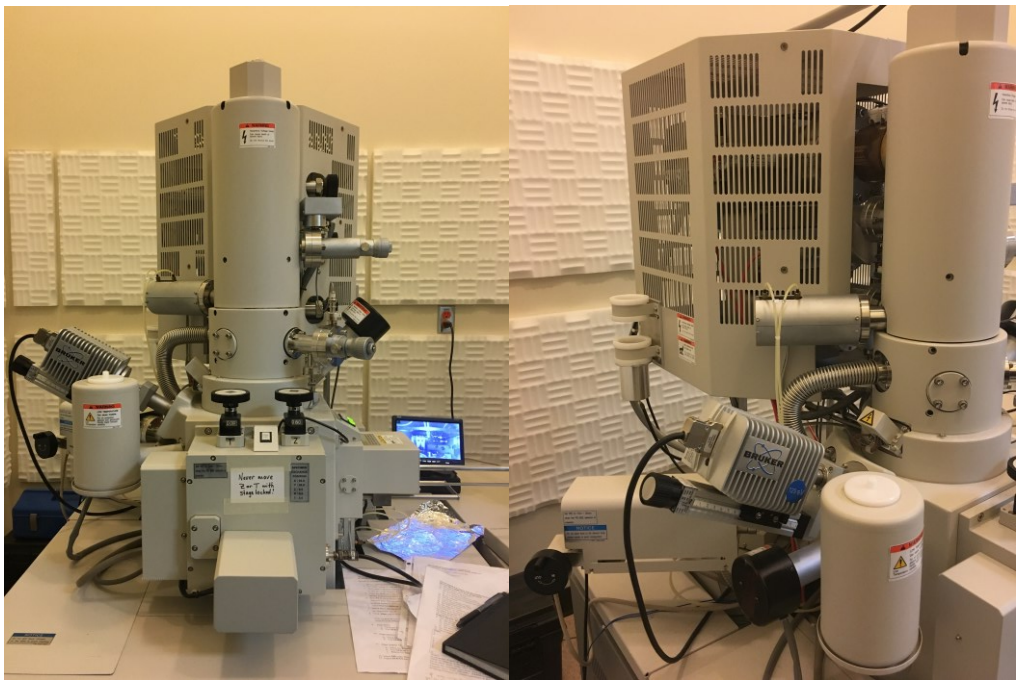

Figure 6: Advanced Microscopy Facility at the University of Victoria

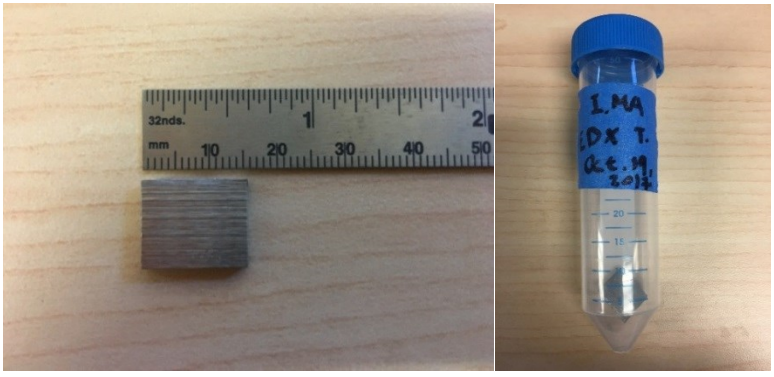

Figure 7: Typical EDX analysis sample

In general, the EDX analysis results agreed well with the mill test reports hence the accuracy of the reports was confirmed. However, similar to the findings in [11], the weight percentages of carbon and boron obtained from the EDX analysis are uncharacteristic for

structural steel and are considered questionable. Hence, this section uses only the results from the mill test reports. It can be seen in Table 3 that all CE-values (from both Equations 1 and 2) are below the 0.44 limit based on the mill test reports. However, it should be noted that for chemical elements not included in the mill test reports, a zero value is assigned in the calculation which may greatly underestimate the CE-values. For RHS 102×102×13, the number of significant figures for the weight percentage of boron is insufficient, since a boron amount of just 0.0003% will cause the CE-values to exceed the limit for Equation 2.

3.3 Geometric measurements

Rigorous measurements on the cross-sectional dimensions were performed on the three parent RHS before mechanical testing. The wall thicknesses at 16 locations around each cross section were measured. The scanned images of the cross sections were imported into AutoCAD. For all corners, the internal and external radii were determined by measuring the radii of the three-point arcs drawn to fit the corners. The averages of the measured thicknesses (t) and the inside corner radii of all measured locations (r_{i1} to r_{i4}) are listed in Table 4. The inside corner radii vary from 1.03t to 1.42t and from 1.38t to 1.66t for RHS 102×102×6.4 and RHS 102×102×7.9, respectively. The corner radii of all corners of RHS 102×102×13 were smaller than the wall thickness. Previous research [31, 32, 51] included measurements on contemporary RHS and reported an internal corner radius ranging from 0.7 to 1.4 times the wall thickness. Some of the corner radii in Table 4 are outside the range. As discussed in Section 2.1.2, the ISO 14346 [34] recommendations on minimum outside corner radii (see Table 1) for welding (in the zones of cold-forming without heat treatment) may be applied to galvanizing for prevention of significant embrittlement [10]. However, this approach is speculative and can be conservative for galvanizing issues [19]. Assuming

that the difference between the outside and inside corner radii is the wall thickness, the recommended minimum inside corner radius is 1.5t for RHS 102×102×6.4 and RHS 102×102×7.9, and 2.0t for RHS 102×102×13. As can be seen in Table 4, most corners of the three parent RHS were cold-formed to degrees that are susceptible to cracking during welding and galvanizing according to the ISO 14346 recommendations.

Table 4: Cross-sectional dimensions of RHS

Parent RHS	t (mm)	r_{i1} (mm)	r_{i2} (mm)	r_{i3} (mm)	r_{i4} (mm)	r_{i1} / t	r_{i2} / t	r_{i3} / t	r_{i4} / t
RHS 102×102×6.4	6.41	7.2	6.6	8.9	9.1	1.12	1.03	1.39	1.42
RHS 102×102×7.9	7.83	11.0	11.9	13.0	10.8	1.40	1.52	1.66	1.38
RHS 102×102×13	12.90	11.8	11.6	11.7	11.9	0.91	0.90	0.91	0.92

3.4 Preparation of specimens

As aforementioned, one of the main objectives of this research is to quantify the changes of material properties and residual stresses at different locations of RHS, due to galvanizing and different degrees of pre-galvanizing heat-treatment. A total of 18 short RHS specimens were prepared from the three parent tubes (see Table 5). Each specimen ID includes three components. The first component (i.e. 6, 8 or 13) is the nominal wall thickness (mm). The second component distinguishes the specimens by different pre-galvanizing treatments, where C = cold-formed (Class C) without any treatment; 450 = cold-formed plus subsequently heat-treated to 450ºC to the Canadian standard for a Class H finish [40] or to ASTM A1085 by specifying Supplement S1 [21]; and 595 = cold-formed plus subsequently heat-treated to an annealing temperature of 595ºC per ASTM A143 [5]. The third component of the ID indicates whether the specimen is galvanized, where U = un-

galvanized; and G = galvanized. For comparison purposes, half of the specimens were galvanized. All galvanized specimens were dipped into the same chemical solutions for surface preparation and later into the molten zinc bath at the same time. Hence, for all galvanized specimens there is no variation in: (1) chemical compositions of surface preparation solutions or zinc bath mixture; and (2) temperature of the molten zinc bath. The hot-dipping process has a duration of 10 minutes.

Table 5: RHS specimens

Parent RHS	#	Specimen ID	Parent RHS	#	Specimen ID	Parent RHS	#	Specimen ID
102×102×6.4	1	6-C-U	102×102×7.9	7	8-C-U	102×102×13	13	13-C-U
	2	6-450-U		8	8-450-U		14	13-450-U
	3	6-595-U		9	8-595-U		15	13-595-U
	4	6-C-G		10	8-C-G		16	13-C-G
	5	6-450-G		11	8-450-G		17	13-450-G
	6	6-595-G		12	8-595-G		18	13-595-G

As discussed in Chapter 2, ASTM A143 [5] suggests a heat treatment at a temperature of 595ºC for 24 min per centimeter of section thickness. On the other hand, CSA G40.20/G40.21 [40] and ASTM A1085 [21] specify only the temperature (450ºC) but not the duration. For comparison purpose, all stress-relieved specimens in this study (i.e. those containing 450 or 595 in their IDs in Table 5) were heat-treated using similar furnace cycles. The furnace cycles began by heating the material from the ambient temperature to the specified temperatures. Once stable at 450ºC or 595ºC, the temperature was held for 30 minutes. The specimens were then cooled in air.

3.5 Microstructure characterization and microcrack detection

Severe cold-forming can sometimes produce crack-like defects on the internal surface of the RHS corner regions. These microcracks may cause stress concentration during hot dip

galvanizing and steels with such defects are susceptible to LME [19]. In this research, detection of microcracks due to cold-forming or galvanizing was performed on the internal surface of the corner regions at the free ends of all 18 RHS specimens in Table 5. Dye penetrant inspections were first performed on the specimens to detect if there were visible cracks to the naked eye. As shown in Figure 8, two pieces of channel-shaped coupons were machined from one free end of the specimens. For all channel-shaped samples, surface cleaning, application of penetrant, removal of excess penetrant, application of developer, and crack inspection were performed per ASTM E165 [52]. No "bleed-out" or indication of visible cracks to the naked eye was found in any of the samples.

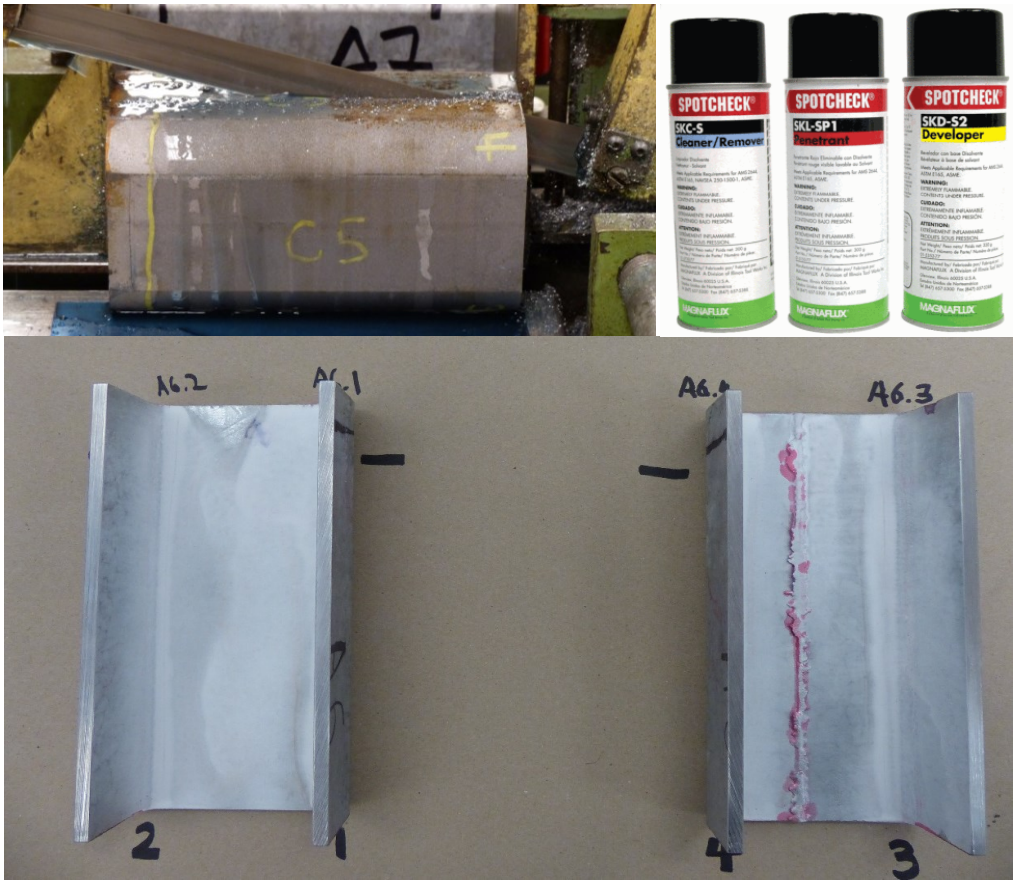

Figure 8: Dye Penetrant Inspection

Although dye penetrant inspections are fast and can be applied to a large surface area, it is possible that the surface cracks are covered by the zinc coating and hence not revealed during the dye penetrant inspections. Hence, for the galvanized RHS specimens metallographic samples were machined, ground, polished and etched per ASTM E3 [53] from the corners at the free end, since experience has shown that cracking in RHS during galvanizing always initiates from the internal corner region at the free end. The samples were polished until "mirror-like" surfaces were obtained. A 2% nital etchant solution was then applied to the surface to remove the hardened layer due to surface polishing (see Figure 9). The primary objective of the metallographic examinations is to reveal the microstructure of the inside surface of the corner regions and to detect microcrack and zinc penetration. All metallographic samples were examined using the microscopy facility shown in Figure 6. Similar to the dye penetrant inspections, although the measured radii of many corners smaller than the minimum values recommended by ISO 14346 [34], no mircocrack or zinc penetration were found from the metallographic examinations.

(a) Etched sample (b) Non-etched sample

Figure 9: Sample after 2% nital etching

3.6 Tensile coupon tests

A total of 108 tensile coupon tests were performed to determine the material properties around the cross sections of the RHS specimens. For each RHS specimen listed in Table 5, two flat tensile coupons from two flat faces away from the weld seam, and four corner coupons were machined and tested following the procedures in ASTM A370 [38]. The locations of coupons on the RHS specimens are shown in Figure 10. The 0.2% strain offset method was applied to determine the yield stress. As suggested by Huang and Young [54] and Ma et al. [55], for testing of corner coupons, a pair of special grips was used to connect the coupon to the universal testing machine (see Figure 11).

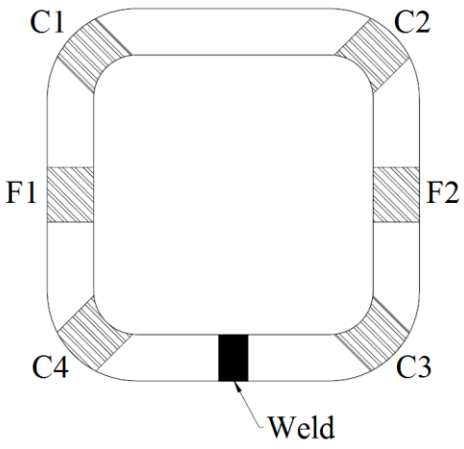

Figure 10: Locations of tensile coupons from RHS specimens

Figure 11: Testing of corner coupons with special grips and pins

3.7 Residual stresses measurement

As discussed in Chapter 2, cracking may initiate from the member free end once the total surface stress (i.e. residual plus thermal) in the member transverse direction (i.e. perpendicular to a longitudinal crack) reaches a critical value. Hence, for severely cold-formed steels it is important to measure the residual stresses at the susceptible locations.

The sectioning method has been used extensively for determination of longitudinal residual stress in hollow sections for structural stability research [27-30, 41], where the measurements were typically taken at a location far away from the member ends. As aforementioned, to this day research on residual stresses (longitudinal and transverse) at the free end of RHS is limited, especially at the corner region in the transverse direction. For determination of residual stresses in different directions on member surface, especially in the transverse direction, the hole-drilling method is recommended [56-58]. In this research, the residual stresses were measured using the hole-drilling method and the standard equipment and strain gauge rosettes recommended in ASTM E837 [10]. The details of residual stress measurements using the hole-drilling method can be found in Section 3.7.1. For measurements in galvanized specimens, the zinc layers were carefully ground off using a sand paper before installation of the strain gauge rosettes. Typical locations of strain gauge rosettes are shown in Figures 12.

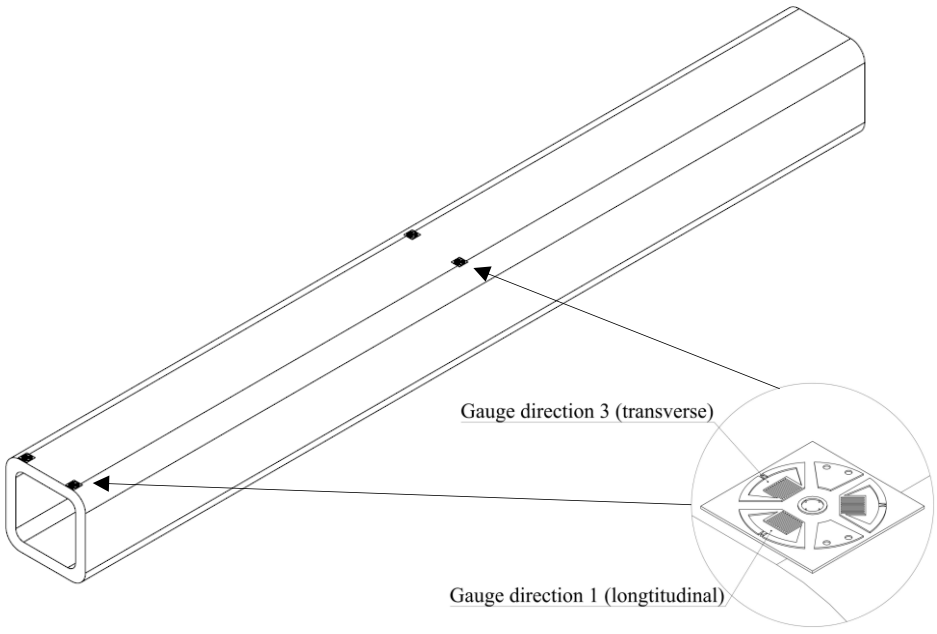

Figure 12: Typical locations of strain gauge rosettes

3.7.1 Test set-up and procedure

To evaluate the effects of different pre-galvanizing heat-treatments per ASTM A143 [5], ASTM A1085 [21] and CSA G40.20/G40.21 [40] to the residual stress properties of RHS 102×102×6.4, 12 strain gauge rosettes were installed at all four corners at the free end of Specimens 6-C-U, 6-450-U and 6-595-U. The same method was applied to RHS 102×102×7.9 and RHS 102×102×13. To determine the residual stress proprieties after galvanizing, four strain gauge rosettes were installed at the same locations on Specimens 8-C-G and 13-C-G.

Figure 13 shows the specialized hole-drilling device used for the residual stress measurement (RS-200 produced by InterTechnology Inc.). The device has the all features required by ASTM E837 [59]. The kit includes: (1) microscope assembly, including an eyepiece, a reticle, and an objective lens for hole alignment; (2) high-speed air turbine assembly used for air-supplied high-speed drilling; and (3) milling rod assembly produced for low speed drilling. It should be noted that ASTM E837 [59] recommends the application of a high-speed air-turbine with rotational speed from 20,000 to 40,000 revolutions per minute for the hole-drilling process, to avoid the machining-induced residual stress by the low-speed drilling. Hence, the assemblies conducted during the test were only the microscope and high-speed air turbine assemblies.

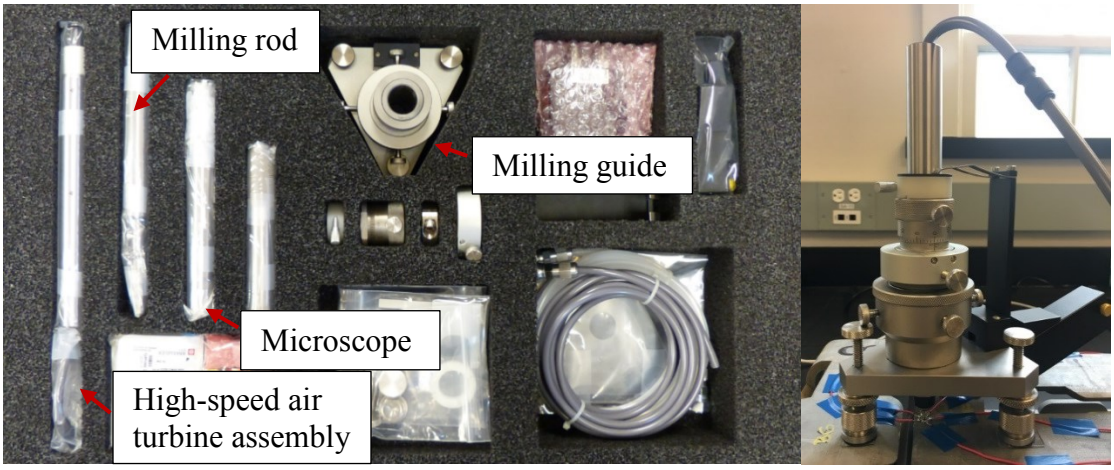

(a) RS-200 Kit

(b) High-speed air turbine assembly

Figure 13: Specialized hole-drilling device

For the strain gauge rosettes, ASTM E837 [59] suggested the use of 1/32 or 1/16 inch Type A (see Figure 14) with a gauge circle diameter of 2.57 or 5.13 mm respectively. It should be noted that the gauge circle diameter should be less than the RHS sample wall thickness [59]. Although both types of strain gauges satisfied the above requirement, 1/16 Type A rosette was selected because it was the most commonly used and recommended by the manufacturer. A 1.6 mm nominal diameter drill-bit was then acquired in compliance with the ASTM E837 [59] requirement on the minimum (1.52 mm) and maximum (2.54 mm) drilled-hole diameter.

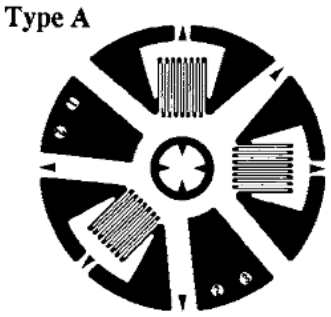

Figure 14: Type A rosette strain gauge [59]

The test procedure using the hle-drilling method were performed in accordance with RS-200 Milling Guide Instruction Manual as follows:

(1) Sample surface preparation including sanding and neutralization.

(2) Installation of strain gauge rosette and soldering.

(3) Mounting RS-200 on the sample surface by using high strength double sided tape.

(4) Hole alignment using the microscope assembly set-up as shown in Figure 15(a).

(5) Zero depth establishing.

(6) Advancing the drill-bit with caution, and taking strain gauge rosette measurements.

(7) Measuring the drilled-hole diameter as shown in Figure 15(b).

(8) Removing the tape and cleaning the station.

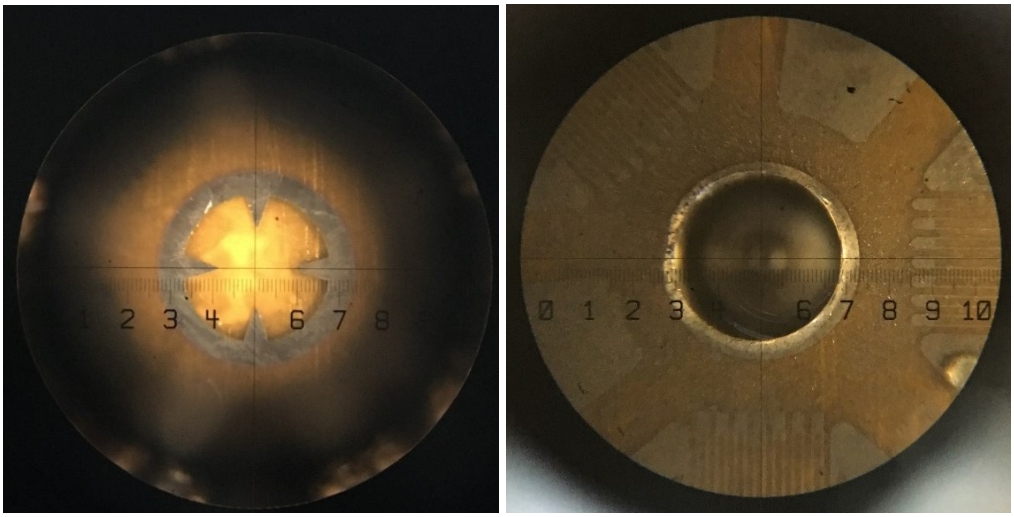

(a) Hole alignment (b) Measuring hole diameter

Figure 15: Gauge hole alignment and drilled-hole diameter measurement

An air power supply regulated at constant pressure (276 kPa) was used during the high-speed drilling process (Step 6), and 10 step-holes were drilled with hole depths of 0.10 mm. The step-hole depths were controlled by the depth setting micrometer within the RS-200 Kit.

It should be noted that all strain gauge rosettes were installed on the flat face adjacent to the corner rather than the curved surface of the corner itself (see Figure 16), since previous research [55] showed that transverse residual stresses at this location were particularly high which could be the driving stress for corner cracking. In addition, the interpretation of results from a strain gauge rosette on a curved surface is extremely difficult and impractical.

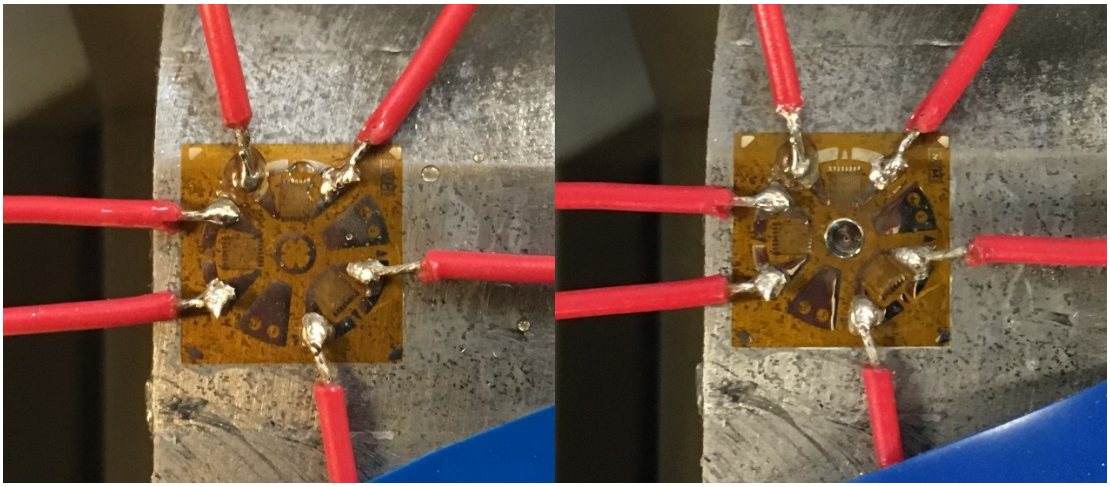

(a) Before the drilling (b) After the drilling

Figure 16: Example of hole-drilling test

All strain gauge rosettes were installed on the external surface of the specimens. For the in-situ residual stress in HSS, extensive experience has shown the bending component is always much larger than the membrane component [27-30, 41, 55]. In this case, the tensile and compressive values on the inside and outside surfaces could approximately be considered equal in magnitude but opposite in sense.

3.7.2 Calculation of Residual stresses

The calculations of residual stresses in the longitudinal and transverse directions were performed using the procedures in ASTM E837 [59]. It should be noted that the calculations were based on the following assumptions: (1) the residual stress was generally

uniform throughout the drilling depth; and (2) the material was homogeneous and isotropic in its mechanical properties, and linear elastic in its stress-strain behavior.

For uniform stresses, thick material, i.e. sample wall thickness larger than the gauge circle. The three parameters, *p, q,* and *t* are introduced by:

$$p = \frac{\varepsilon_3 + \varepsilon_1}{2} \tag{3}$$

$$q = \frac{\varepsilon_3 - \varepsilon_1}{2} \tag{4}$$

$$t = \frac{\varepsilon_3 + \varepsilon_1 - 2\varepsilon_2}{2} \tag{5}$$

Where $\varepsilon_{1,2,and\ 3}$ are the relieved strain measured after the drilling process.

The three combination stresses *P*, *Q*, and *T* then can be determined as:

$$P = \frac{\sigma_y + \sigma_x}{2} = -\frac{Ep}{a(1+\nu)} \tag{6}$$

$$Q = \frac{\sigma_y - \sigma_x}{2} = -\frac{Eq}{b} \tag{7}$$

$$T = \tau_{xy} = -\frac{Et}{b} \tag{8}$$

Where:

P = isotropic, or equi-biaxial stress;

Q = 45° shear stress;

T = xy shear stress;

a and *b* = calibration constant for isotropic and shear stress.

Constants *a* and *b* are factors specified in ASTM E837 [59] for standard hole-drilling device and strain gauge rosettes used in this research. The constants can also be determined by experimental calibration if non-standard device or rosette is used (e.g. [57]).

The Cartesian stresses σ_x, σ_y, and τ_{xy} then can be determined:

$$\sigma_x = P - Q, \qquad \sigma_y = P + Q, \qquad \tau_{xy} = T \tag{9}$$

The principal stresses can be calculated:

$$\sigma_{max}, \sigma_{min} = P \pm \sqrt{Q^2 + T^2} \tag{10}$$

And the corresponding direction angle β is:

$$\beta = \frac{1}{2}\arctan(\frac{-T}{-Q}) \tag{11}$$

4.0 Results and discussions

4.1 Material strength and ductility

Typical tensile stress-strain curves are shown in Figure 17(a) and (b). For the corner coupons, the key test results (f_y, f_u and percentage elongation at fracture) are plotted in Figures 18(a) to (c) against the normalized corner radii from Table 4. The averages of the key test results for the 18 RHS subjected to different treatments are listed in Tables 6(a) to (c). Similarly, the test results of the flat coupons are presented in Figures 19(a) to (c) and Tables 7(a) to (c). Tables 6 and 7 also include the changes in material properties due to heat treatment or galvanizing (by comparing to the cold-formed ungalvanized (C-U) base material).

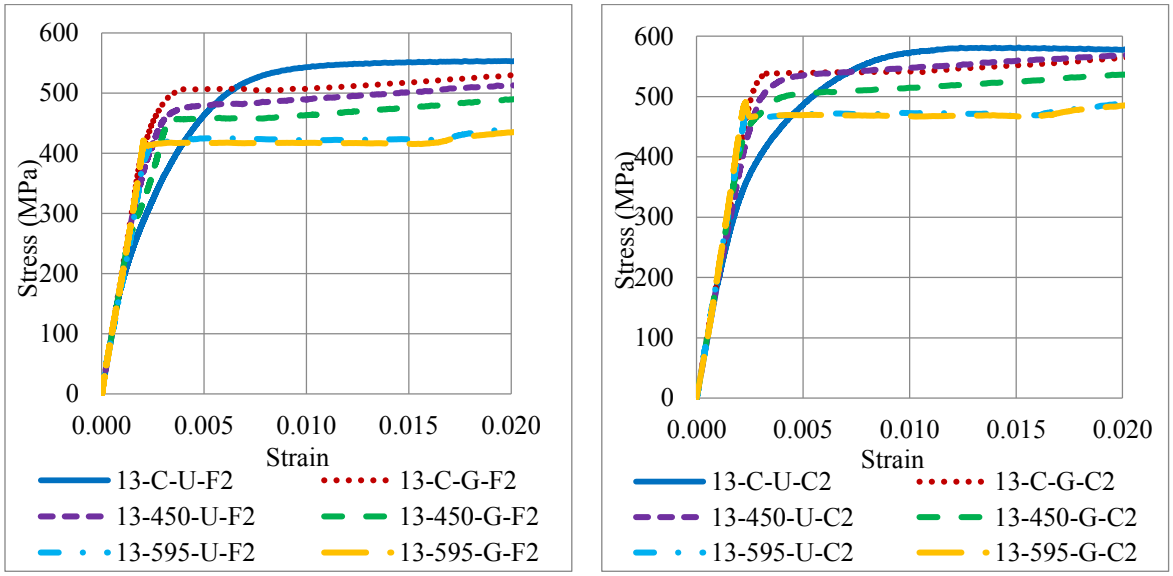

(a) Flat coupons from RHS 102×102×13 (b) Corner coupons from RHS 102×102×13

Figure 17: Typical tensile stress-strain curves

By comparing the typical tensile stress-strain curves of the flat coupons from 13-C-U, 13-450-U and 13-595-U in Figure 17(a), the proportional limit stress increases as the heat treatment temperature increases. It can also been seen from Figure 17(a) that the curves of flat coupons from 13-450-U and 13-C-G are very close to each other. Hence, the decreases

in residual stress and the increases in material yield strength as a result of the 30-minute 450ºC Class H heat treatment and the 10-minute hot dipping process can sometimes be comparable. On the other hand, by comparing 13-450-U to 13-450-G and 13-595-U to 13-595-G in Figure 17(a), the hot dipping process resulted in negligible changes in the tensile stress-strain behaviours of pre-galvanizing heat-treated specimens. Similar observations can be made from the corner coupon curves shown in Figure 17(b).

The following observations could be made from the corner coupon test results in Figure 18 and Table 6:

(1) The 450ºC heat treatment has increased the yield and ultimate strengths of corner materials of RHS 102×102×6.4 by 11% and 12%, respectively. For the same holding time in the furnace (30 minutes), the strength increase as a result of the 450ºC treatment becomes smaller as wall thickness increases from 6.4 mm to 7.9 mm and becomes negligible when the wall thickness becomes 13 mm.

(2) Different from the 450ºC heat treatment, the 595ºC heat treatment has decreased the yield (up to 13%) and ultimate (up to 8%) strengths of corner materials for all three sizes of parent tubes. Similarly, for the same holding time in the furnace (30 minutes) the change in material strength becomes smaller as the RHS wall thickness increases.

(3) For RHS with a nominal wall thickness of 13 mm, the changes on the yield and ultimate strengths of the corner material due to the hot-dip galvanizing process are comparable to those from the 450ºC heat treatment. However, in general the galvanizing process does not increase significantly the strength of the corner material, regardless of whether the material has been subject to pre-galvanizing heat-treatment (e.g. 6-C-U versus 6-C-G) or not (e.g. 6-450-U versus 6-450-G, and 6-595-U versus 6-595-G).

(4) The 595ºC heat treatment improves significantly the ductility of the corner material. However, there is a trade-off between material strength and ductility. On the other hand, both the 450ºC heat treatment and the galvanizing processes can effectively improve the ductility with no strength reduction.

The following observations could be made from the flat coupon test results in Figure 19 and Table 7:

(1) Comparing to the corner material, the galvanizing process and the 450ºC heat treatment led to smaller increases in the yield (up to 7%) and ultimate strengths (up to 6%) of flat face materials for all sizes of cross-sections.

(2) Similar to the corner material, the 595ºC heat treatment lowered the yield strengths (up to 11%) and the ultimate strength (up to 4%) of the flat face material.

(3) For the materials subject to pre-galvanizing heat-treatments, the hot-dipping process has negligible effects on the flat face material properties.

(4) Comparing to the corner coupon test results, the improvement of material ductility at the flat faces due to galvanizing and heat treatment to different degrees are smaller.

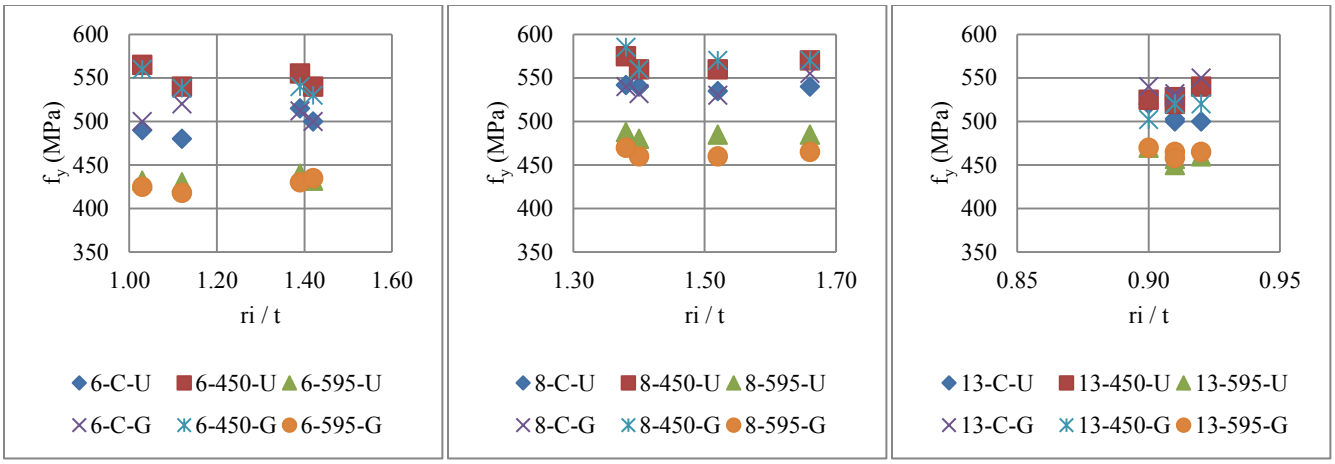

(a) Yield strength

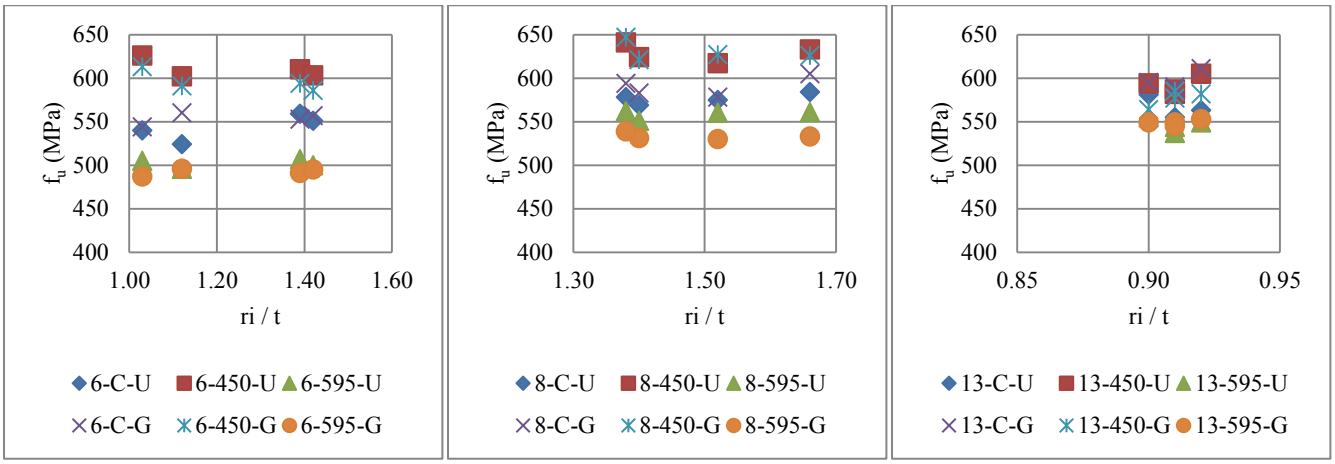

(b) Ultimate strength

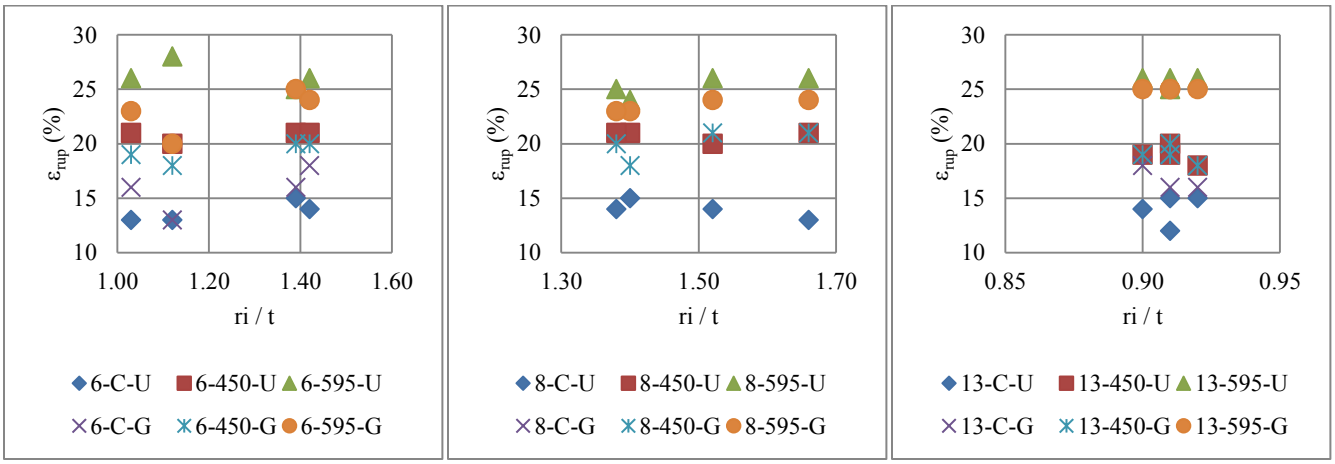

(c) Percentage elongation at fracture

Figure 18: Key tensile test results of corner coupons

Table 6: Averages of tensile test results of corner coupons

Specimen ID	$f_{yc,avg}$ (MPa)	Change in $f_{yc,avg}$ due to heat treatment or galvanizing	$f_{u,avg}$ (MPa)	Change in $f_{uc,avg}$ due to heat treatment or galvanizing	ε_{rup}	Change in ε_{rup} due to heat treatment or galvanizing
6-C-U	496	–	544	–	14%	–
6-450-U	550	+11%	610	+12%	21%	+50%
6-595-U	434	-13%	502	-8%	26%	+86%
6-C-G	508	+2%	554	+2%	16%	+14%
6-450-G	542	+9%	596	+10%	19%	+36%
6-595-G	427	-14%	492	-10%	23%	+64%

(a) RHS 102×102×6.4

Specimen ID	$f_{yc,avg}$ (MPa)	Change in $f_{yc,avg}$ due to heat treatment or galvanizing	$f_{u,avg}$ (MPa)	Change in $f_{uc,avg}$ due to heat treatment or galvanizing	ε_{rup}	Change in ε_{rup} due to heat treatment or galvanizing
8-C-U	539	–	577	–	14%	–
8-450-U	566	+5%	629	+9%	21%	+50%
8-595-U	485	-10%	559	-3%	25%	+79%
8-C-G	539	0%	590	+2%	17%	+21%
8-450-G	571	+6%	630	+9%	20%	+43%
8-595-G	464	-14%	533	-8%	24%	+71%

(b) RHS 102×102×7.9

Specimen ID	$f_{yc,avg}$ (MPa)	Change in $f_{yc,avg}$ due to heat treatment or galvanizing	$f_{u,avg}$ (MPa)	Change in $f_{uc,avg}$ due to heat treatment or galvanizing	ε_{rup}	Change in ε_{rup} due to heat treatment or galvanizing
13-C-U	506	–	563	–	14%	–
13-450-U	528	+4%	592	+5%	19%	+36%
13-595-U	459	-9%	546	-3%	26%	+86%
13-C-G	538	+6%	596	+6%	17%	+21%
13-450-G	516	+2%	577	+2%	19%	+36%
13-595-G	465	-8%	549	-2%	25%	+79%

(c) RHS 102×102×13

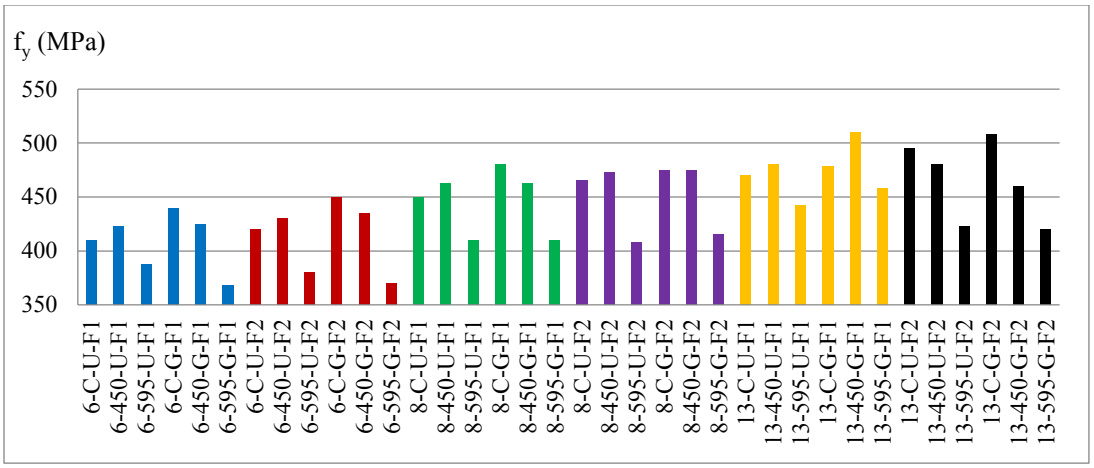

(a) Yield strength (f_y)

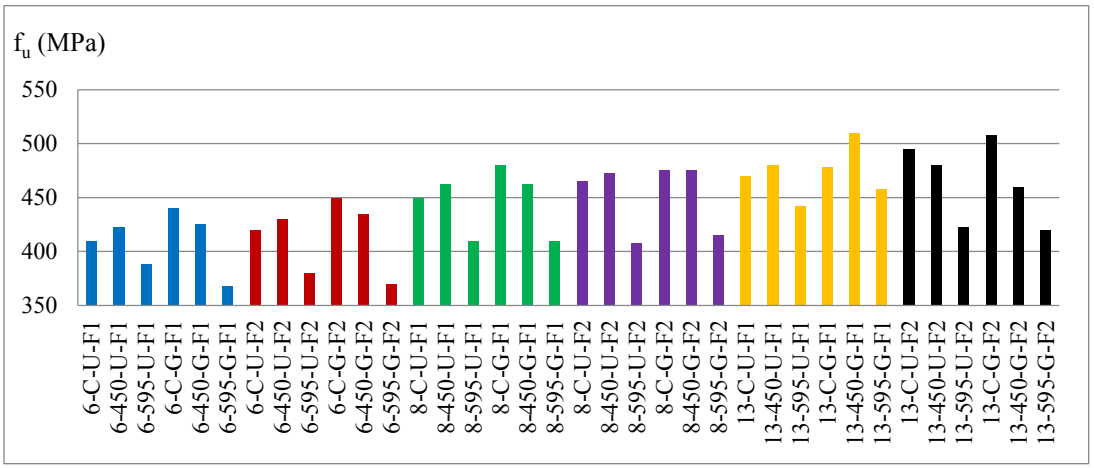

(b) Ultimate strength (f_u)

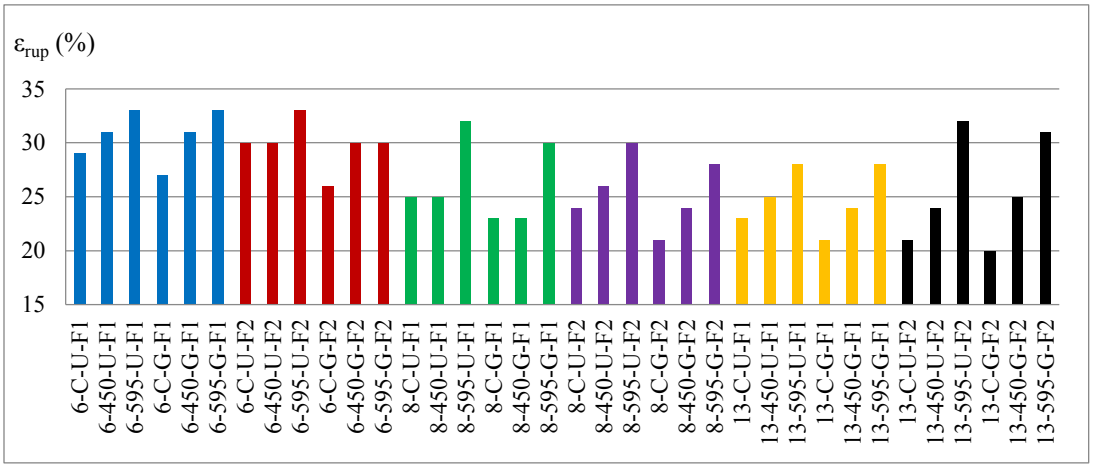

(c) Percentage elongation at fracture (ε_{rup})

Figure 19: Key tensile test results of flat coupons

Table 7: Averages of tensile test results of flat coupons

Specimen ID	$f_{yf,avg}$ (MPa)	Change in $f_{yf,avg}$ due to heat treatment or galvanizing	$f_{u,avg}$ (MPa)	Change in $f_{u,avg}$ due to heat treatment or galvanizing	ε_{rup}	Change in ε_{rup} due to heat treatment or galvanizing
6-C-U	415	–	482	–	30%	–
6-450-U	427	+3%	505	+5%	31%	+3%
6-595-U	384	-7%	486	+1%	33%	+10%
6-C-G	445	+7%	509	+6%	27%	-10%
6-450-G	430	+4%	502	+4%	31%	+3%
6-595-G	369	-11%	447	-7%	32%	+7%

(a) RHS 102×102×6.4

Specimen ID	$f_{yf,avg}$ (MPa)	Change in $f_{yf,avg}$ due to heat treatment or galvanizing	$f_{u,avg}$ (MPa)	Change in $f_{uf,avg}$ due to heat treatment or galvanizing	ε_{rup}	Change in ε_{rup} due to heat treatment or galvanizing
8-C-U	458	–	509	–	25%	–
8-450-U	468	+2%	539	+6%	26%	+4%
8-595-U	409	-11%	505	-1%	31%	+24%
8-C-G	478	+4%	530	+4%	22%	-12%
8-450-G	469	+2%	538	+6%	24%	-4%
8-595-G	413	-10%	501	-2%	29%	+16%

(b) RHS 102×102×7.9

Specimen ID	$f_{yf,avg}$ (MPa)	Change in $f_{yf,avg}$ due to heat treatment or galvanizing	$f_{u,avg}$ (MPa)	Change in $f_{uf,avg}$ due to heat treatment or galvanizing	ε_{rup}	Change in ε_{rup} due to heat treatment or galvanizing
13-C-U	483	–	549	–	22%	–
13-450-U	480	-1%	566	+3%	25%	14%
13-595-U	433	-10%	527	-4%	30%	36%
13-C-G	493	+2%	555	+1%	21%	-5%
13-450-G	485	0%	559	+2%	25%	14%
13-595-G	439	-9%	527	-4%	30%	36%

(c) RHS 102×102×13

4.2 Residual stresses in different directions and at different locations

The results from the 40 strain gauge rosettes were normalized by the average of yield strengths of the two flat coupons ($f_{yf,avg}$) from the cold-formed and ungalvanized base specimens and plotted in Figures 20(a) and (b) against the normalized inside corner radii. The averages of the measured longitudinal ($\sigma_{rs,long,avg}$) and transverse ($\sigma_{rs,long,avg}$) residual stresses are normalized by $f_{yf,avg}$ in Table 8 . Table 8 also includes the changes in residual stresses due to heat treatment or galvanizing (by comparing to the cold-formed ungalvanized (C-U) base material). To quantify the difference in residual stresses at the free end and the middle of the specimens, an additional 8 strain gauge rosettes were installed at the middle of Specimens 8-C-U, 8-C-G, 13-C-U and 13-C-G. The comparisons of the measured values are shown in Figures 21(a) and (b). The comparisons of the average values are shown in Table 9.

The data at all measuring points at the free end of the specimens are shown in Figures 21(a) and (b). It can be seen that both heat treatment and galvanizing not only lowered the magnitude but also smoothed the distribution of residual stress at different corners for specimens of different cross-sectional dimensions. In general the longitudinal residual stresses are higher than the transverse ones. For the ungalvanized cold-formed specimens (i.e. 6-C-U, 8-C-U and 13-C-U), the longitudinal residual stresses at the free end range from 33% to 54% of $f_{yf,avg}$, and the transverse residual stresses range from 20% to 39% of $f_{yf,avg}$. One important finding is that the residual stresses in the transverse direction at the free end of the measured specimens are in general within the same order of magnitude of the thermal stress in the same direction during the hot dipping process (see Chapter 2). The thermal stress in the extreme cases (up to 400 MPa) can be higher than the residual stress.

The following observations could be made from the averages of the data at the free end of the specimens are shown in Table 8:

(1) By comparing 13-C-U to 13-595-U, the 595ºC heat treatment [5] reduces significantly the residual stresses generated from cold-forming. A 69% decrease in longitudinal residual stress and a 66% decrease in transverse residual stress were observed. Similar observations can be made on the specimens with nominal wall thicknesses of 6.4 mm and 7.9 mm.

(2) By comparing 13-C-U to 13-450-U, a 34% decrease in longitudinal residual stress and a 31% decrease in transverse residual stress were observed. Similar observations can be made on the specimens with nominal wall thicknesses of 6.4 mm and 7.9 mm. It can be seen that the 450 ºC heat treatment [21, 40] is a lot less effective in relieving the residual stresses comparing to the ASTM A143 heat treatment at 595ºC. Also, the 595ºC is more effective in improving the material ductility. This explains why experience in Canada [10] has shown that corner cracking can still occur with CAN/CSA-G40.20/G40.21Class H RHS [21]. However, it should be noted that, as mentioned in Section 4.1, the 595ºC heat treatment could sometimes significantly decrease the material strength.

(3) By comparing 13-450-U to 13-C-G, it can be seen that hot dipping the RHS material in a molten zinc bath maintained at 450ºC for a much shorter period of time (i.e. 10 minutes) provides a partial residual stress relief comparable to the 450 ºC heat treatment [21, 40]. Similar observations can be made on the specimens with a nominal wall thickness of 7.9 mm. Hence, the effects of the galvanizing process on the residual stress properties of cold-formed hollow section material should not be neglected. Further research is needed on the optimized duration of heat treatment to different degrees.

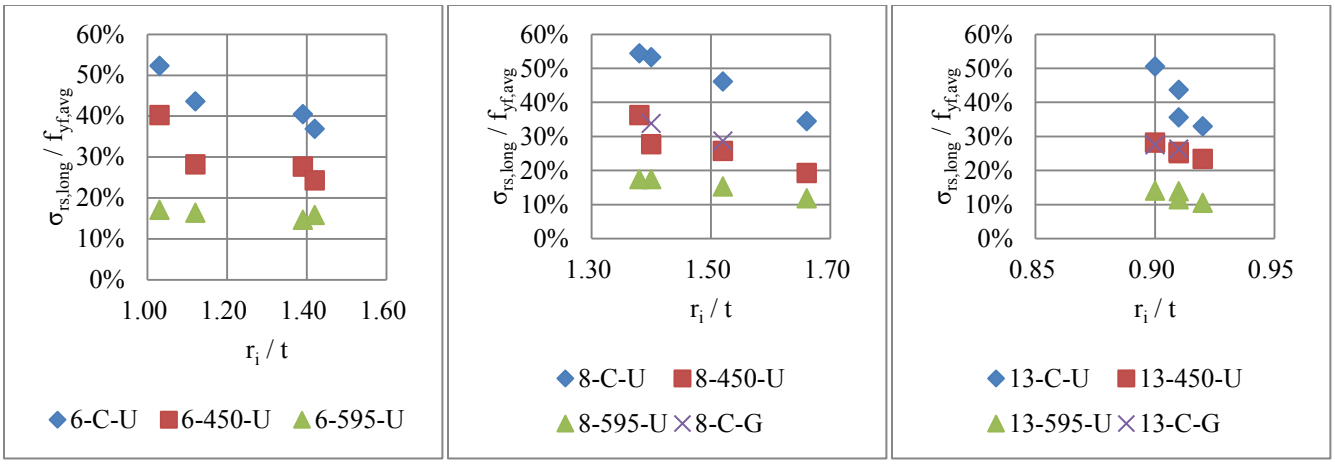

(a) Longitudinal residual stresses

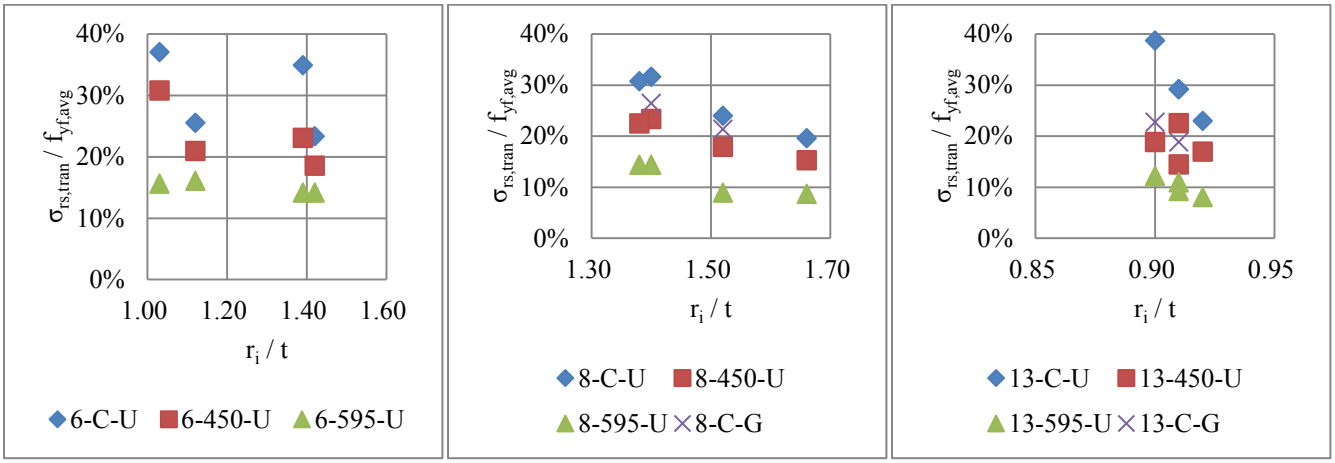

(b) Transverse residual stresses

Figure 20: Measured residual stresses at the free end

Table 8: Normalized values of residual stresses at the free end

Specimen ID	$\sigma_{rs,long,avg} / f_{yf,avg}$	Change in $\sigma_{rs,long,avg}$ due to heat treatment or galvanizing	$\sigma_{rs,tran,avg} / f_{yf,avg}$	Change in $\sigma_{rs,tran,avg}$ due to heat treatment or galvanizing
6-C-U	43%	–	30%	–
6-450-U	30%	-30%	23%	-23%
6-595-U	16%	-63%	15%	-50%

(a) RHS 102×102×6.4

Specimen ID	$\sigma_{rs,long,avg} / f_{yf,avg}$	Change in $\sigma_{rs,long,avg}$ due to heat treatment or galvanizing	$\sigma_{rs,tran,avg} / f_{yf,avg}$	Change in $\sigma_{rs,tran,avg}$ due to heat treatment or galvanizing
8-C-U	47%	–	27%	–
8-450-U	27%	-42%	20%	-26%
8-595-U	16%	-67%	12%	-56%
8-C-G	31%	-34%	24%	-10%

(b) RHS 102×102×7.9

Specimen ID	$\sigma_{rs,long,avg} / f_{yf,avg}$	Change in $\sigma_{rs,long,avg}$ due to heat treatment or galvanizing	$\sigma_{rs,tran,avg} / f_{yf,avg}$	Change in $\sigma_{rs,tran,avg}$ due to heat treatment or galvanizing
13-C-U	41%	–	30%	–
13-450-U	26%	-37%	18%	-39%
13-595-U	13%	-69%	10%	-66%
13-C-G	27%	-34%	21%	-31%

(c) RHS 102×102×13

The normalized values of residual stresses at the free end and the middle of some specimens are listed in Table 9. By comparing the data from 8-C-U and 13-C-U, it can be seen that the residual stresses (both longitudinal and transverse) at the free end are a lot lower than those at the middle. The galvanizing process relieves effectively the residual stress at both the free end and the middle of the specimen. However, the correlations between residual stresses at different locations and the cross-sectional dimensions are not clear based on limited amount of data. Hence, further research is needed in this regard.

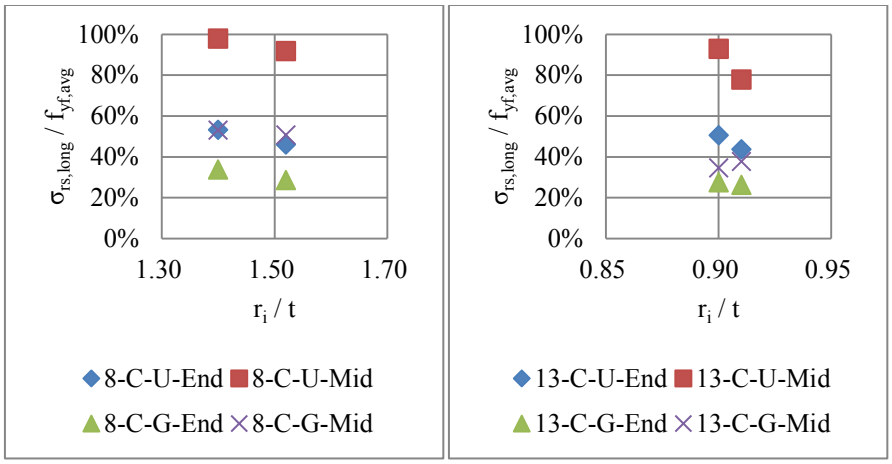

(a) Longitudinal residual stresses

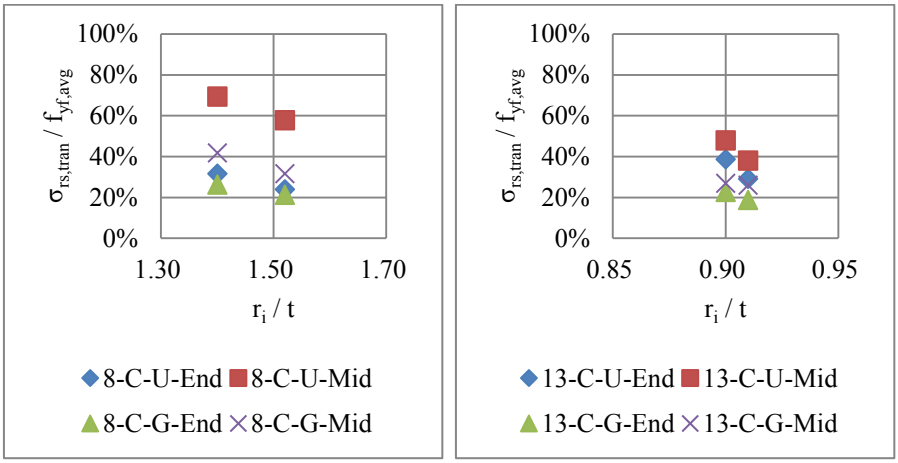

(b) Transverse residual stresses

Figure 21: Comparison of measured residual stresses at the middle and free-end

Table 9: Comparisons of normalized values of residual stresses at the free end and the middle of specimens

Specimen ID	Location	$\sigma_{rs,long,avg} / f_{yf,avg}$	$\sigma_{rs,tran,avg} / f_{yf,avg}$
8-C-U	End	50%	28%
	Middle	95%	64%
8-C-G	End	31%	24%
	Middle	52%	37%
13-C-U	End	47%	34%
	Middle	85%	43%
13-C-G	End	27%	21%
	Middle	36%	27%

5.0 Conclusions

This research sought to: (1) provide a basis for understanding the corner cracking phenomenon in galvanized rectangular hollow sections (RHS); and (2) facilitate the applications of galvanized and heat-treated hollow section materials. Hence, the effects of different fabrication processes on the material and residual stress properties of 18 RHS specimens were investigated via tensile coupon tests and residual stress measurements using the hole-drilling method. In particular, this research for the first time studied comprehensively the residual stresses in the corner regions at the member free ends, since residual stresses at these locations are directly relevant to cracking during galvanizing. Based on the material tested, it was found that:

(1) Although many of the RHS specimens have corner radii smaller than the minimum values per ISO 14346 [34], no microcrack was found in the ungalvanized and galvanized specimens. It should be noted that the ISO 14346 recommendations are intended for prevention of significant embrittlement during welding (in the zones of cold-forming without heat treatment). Hence, further research is needed for development of crack prevention rules catering to galvanizing.

(2) The galvanizing process improved the ductility of the tested cold-formed material. It also led to a minor increase in yield strength.

(3) The effects of hot-dip galvanizing process on the residual stress properties should not be neglected. Hot dipping the RHS material in a molten zinc bath maintained at 450ºC for 10 minutes provided a partial residual stress relief comparable to a 450ºC heat treatment with a 30-minute holding time. Further research is needed to determine the optimized heat treatment duration for a partial residual stress relief for improvement of column behaviour.

(4) The 595ºC heat treatment significantly lowered the residual stress and improved the ductility of the corner material. On the other hand, the 450ºC heat treatment is less effective, which explains why experience in Canada [10] has shown that corner cracking can still occur with CAN/CSA-G40.20/G40.21 Class H RHS [40]. However, there is a trade-off between material strength and ductility for the 595ºC heat treatment.

.

References

[1] AGA, "Hot-dip galvanizing for corrosion protection – a specifiers guide," American Galvanizers Association, Centennial, USA, 2006.

[2] Packer, J.A., Henderson JE. Hollow structural section connections and trusses – a design guide, 2nd ed., Toronto, Canada: Canadian Institute of Steel Construction, 1997.

[3] Kinstler, T.J., "Current knowledge of the cracking of steels during galvanizing – a synthesis of the available technical literature and collective experience for the American Institute of Steel Construction," GalvaScience LLC, Springville, USA, 2005.

[4] ASTM, Standard practice for providing high-quality zinc coating (hot-dip), ASTM A385/A385M-15, West Conshohocken, USA: American Society for Testing and Materials, 2015.

[5] ASTM, Standard practice for safeguarding against embrittlement of hot-dip galvanized structural steel products and procedure for detecting embrittlement, ASTM A143/A143M-07, West Conshohocken, USA: American Society for Testing and Materials, 2014.

[6] ASTM, Standard practice for safeguarding against warpage and distortion during hot-dip galvanizing of steel assemblies, ASTM A384/A384M-07, West Conshohocken, USA: American Society for Testing and Materials, 2013.

[7] AS/NZS, "Hot-dip galvanized (zinc) coatings on fabricated ferrous articles," Standards Australia and Standards New Zealand, Sydney, Australia and Wellington, New Zealand, 2006.

[8] BCSA/GA, "Galvanizing structural steelwork – an approach to the management of liquid metal assisted cracking," British Constructional Steelwork Association, West Midlands, UK, 2005.

[9] ISO, "Zinc coating – guidelines and recommendations for the protection against corrosion of iron and steel in structures – part 2: hot dip galvanizing, ISO 14713-2:2009," International Organization for Standardization, Geneva, Switzerland, 2009.

[10] Packer, J.A., Chiew, S.P., Tremblay, R., Martinez-Saucedo, G., "Effect of material properties on hollow section performance," *Structures and Buildings,* vol. 163, no. SB6, pp. 375-390, 2010.

[11] DiGiovanni C., Li, L., Driver, R., Callele, L., "Cracking in welded steel platform structures during hot-dip galvanization," *Engineering Failure Analysis,* vol. 79, pp. 1031-1042, 2017.

[12] Foley, C.M., Diekfuss, J.A. and Wan, B., "Fatigue risks in the connections of sign supporting structures," Wisconsin Department of Transportation Report No. WHRP 0092-09-07, Department of Civil and Environmental Engineering, Marquette University, Milwaukee, USA, 2013.

[13] Goyal, R., Dhonde, H.B., Dawood, M., "Fatigue failure and cracking in high mast poles," Texas Department of Transportation Report No. FHWA/TX-12/0-6650-1,

Department of Civil and Environmental Engineering, University of Houston, Houston, USA, 2012.

[14] Ocel, J.M., "Fatigue testing of galvanized and ungalvanized socket connections. Federal Highway Administration Report No. FHWA-HRT-14-066," Federal Highway Administration, McLean, USA, 2014.

[15] Stem, A., Richman, N., Pool, C., Rios, C., Anderson, T., Frank, K. , "Fatigue life of steel base plate to pole connection for traffic structures. Texas Department of Transportation Report FHWA/TX-11/9-1526-1," Center for Transportation Research, University of Texas at Austin, Austin, USA, 2011.

[16] Feldmann, M., Pinger, T., Schafer, D., Pope, R., Smith, W., Sedlacek, G., "Hot-dip-zinc-coating of prefabricated structural steel components," JRC Scientific and Technical Research Report No. 56810, European Commission Joint Research Centre, Luxembourg, 2010.

[17] Shi, G., Xue, J., Zhou, W., Chan, T.M., Zhang, Y., "Experimental investigation and modeling on residual stress of welded steel circular tubes," *International Journal of Steel Structures,* vol. 13, no. 3, pp. 595-508, 2013.

[18] Shi, G., Xue, J., Zhou, W., Zhang, Y., "Experimental study on overall buckling behavior of Q420 high strength welded galvanized tubes under axial compression," *Journal of Harbin Institute of Technology,* vol. 45, no. 10, pp. 70-85, 2013.

[19] Sun, M., Packer, J.A., "Hot-dip galvanizing of cold-formed steel hollow sections: a state-of-the-art review," *Frontiers of Structural and Civil Engineering,* 2017.

[20] Poag, G., Zervoudis, J., "Influence of various parameters on steel cracking during galvanizing," in *AGA TechForum*, Kansas, USA, 2003.

[21] ASTM, Standard specification for cold-formed welded carbon steel hollow structural sections (HSS), ASTM A1085/A1085M-15, West Conshohocken, USA: American Society for Testing and Materials, 2015.

[22] JSA, "High tensile strength steel for tower structural purposes, JIS G3129:2005," Japan Standards Association, Tokyo, Japan, 2005.

[23] CEN, "Hot finished structural hollow sections of non-alloy and fine grain steels – part 1: technical delivery conditions, EN 10210-1:2006(E)," European Committee for Standardization, Brussels, Belgium, 2006.

[24] CEN, "Hot finished structural hollow sections of non-alloy and fine grain steels – part 2: tolerances, dimensions and sectional properties, EN 10210-1:2006(E)," European Committee for Standardization, Brussels, Belgium, 2006.

[25] ASTM, Standard specification for hot-formed welded and seamless carbon steel structural tubing, ASTM A501/A501M-14, West Conshohocken, USA: American Society for Testing and Materials, 2014.

[26] Sun M, Packer J.A., "Direct forming versus continuous forming, for cold-formed square hollow sections," in In: Proceedings of the 14th. International Symposium on Tubular Structures, London, UK, 2012.

[27] Davison, T.A., Birkemoe, P.C., "Column behaviour of cold-formed hollow structural steel shapes," *Canadian Journal of Civil Engineering,* no. 10(1):125-141, 1983.

[28] Key, P.W., Hancock, G.J., "A theoretical investigation of the column behaviour of cold-formed square hollow sections," *Thin-Walled Structures,* vol. 16, no. 1, pp. 31-64, 1993.

[29] Gardner, L., Saari, N., Wang, F., "Comparative experimental study of hot-rolled and cold-formed rectangular hollow sections," *Thin-Walled Structures,* vol. 48, no. 7, pp. 495-507, 2010.

[30] Tong, L.W., Hou, G., Chen, Y.Y., Zhou, F., Shen, K., Yang, A., "Experimental investigation on longitudinal residual stresses for cold-formed thick-walled square hollow sections," *Journal of Constructional Steel Research,* vol. 73, pp. 105-116, 2012.

[31] Sun, M., Packer, J.A., "Direct-formed and continuous-formed rectangular hollow sections – comparison of static properties," *Journal of Constructional Steel Research,* vol. 92, pp. 67-78, 2014.

[32] Sun, M., Packer, J.A., "Charpy V-notch impact toughness of cold-formed rectangular hollow sections," *Journal of Constructional Steel Research,* vol. 97, pp. 114-126, 2014.

[33] Sedlacek, G., Feldmann, M., Kuhn, B., Tschickardt, D., Hohler, S., Muller, C., Hensen, W., Stranghoner, N., Dahl, W., Langenberg, P., Munstermann, S., Brozetti, J., Raoul, J., Pope, R., Bijlaard, F., "Commentary and worked examples to EN 1993-1-10 "Material toughness and through thickness properties" and other thoughness oriented rules in EN 1993," JRC Scientific and Policy Rpoert No. 47278, European Commission Joint Research Centre, Luxembourg, 2008.

[34] ISO, "Static design procedure for welded hollow-section joints – recommendations, ISO 14346:2013," International Organization for Standardization, Geneva, Switzerland, 2013.

[35] CECS, Technical specification for structures with steel hollow sections, Beijing, China: China Association for Engineering Construction Standardization, 2010.

[36] CEN, "Cold formed welded structural hollow sections of non-alloy and fine grain steels – part 1: technical delivery conditions, EN 10219-1:2006(E)," European Committee for Standardization, Brussels, Belgium, 2006.

[37] AS/NZS, "Cold-fromed structural steel hollow sections," Standards Australia and Standards New Zealand, Sydney, Australia and Wellington, New Zealand, 2016.

[38] ASTM, Standard test methods and definitions for mechanical testing of steel products, ASTM A370-17, West Conshohocken, USA: American Society for Testing and Materials, 2017.

[39] SAC, "Metallic coatings – hot dip galvanized coatings on fabricated iron and steel articles – specifications and test methods, GB/T 13912-2002," Standardization Administration of the People's Republic of China, Beijing, China, 2002.

[40] CSA, "General requirements for rolled or welded structural quality steel/structural quality steel, CAN/CSA-G40.20-13/G40.21-13," Canadian Standards Association, Toronto, Canada, 2013.

[41] Somodi, B., Kovesdi, B., "Residual stress measurements on cold-formed HSS hollow section columns," *Journal of Constructional Steel Research,* vol. 128, pp. 706-720, 2017.

[42] Kikuchi M., Iezawa T., "Effect of stress-concentration on liquid metal embrittlement cracking of steel by molten zinc," Journal of the Society of Materials Science,Japan, vol. 31, no. 342, pp. 271-276, 1982.

[43] Kominami, Y., Yano, K., Ishimoto, K., Terasaki, T., Mukae, S., "Thermal stress of plate and pipe occurred during dipping in the molten zinc bath – liquid metal embrittlement of welded joint of steel during hot dip galvanizing (report 2).," *Quarterly Journal of the Japan Welding Society,* vol. 3, no. 2, pp. 347-352, 1985.

[44] Vander Voort, G.F., "Embrittlement of Steels," in *ASM Handbook, Volume 01 - properties and selection: irons, steels, and high-performance alloys*, Geauga County, USA, ASM International, 1990., pp. 689-736.

[45] Krauss, G., Steels - processing, structure, and performance, 2nd ed., Geauga County, USA: ASM International, 2015.

[46] Zervoudis, J., Anderson, G., "A review of bath alloy additives and their impact on the quality of galvanized coating," in *6th. Asia Pacific General Galvanizing Conference*, Cairns, Australia, 2005.

[47] Gagne, M., "Industrial testing of zinc-bismuth alloys for after-fabrication hot dip galvanizing," in *18th. International Galvanizing Conference*, Birmingham, UK, 1997.

[48] Gilles, M., Sokolowski, R., "The zinc-tin galvanizing alloy: a unique zinc alloy for galvanizing any reactive steel grade," in *18th. International Galvanizing Conference*, Birmingham, UK, 1997.

[49] Pankert, R., Dhaussy, D., Beguin, P., Gilles, M., "Three years industrial experience with the galveco alloy," in *20th. International Galvanizing Conference*, Amsterdam, Netherlands, 2003.

[50] Nyrstar, "Annual report 2008," Nyrstar, Balen, Belgium, 2008. [Online]. Available: http://www.nyrstar.com/investors/en/Nyr_Documents/English/Nyrstar_Annual_Report-FINAL_(EN).pdf.

[51] Packer, J.A., "Frater GS. Recommended effective throat sizes for flare groove welds to HSS," *Engineering Journal,* vol. 42, no. 1, pp. 31-44, 2005.

[52] ASTM, Standardpractice for liquid penetrant examination for general industry, ASTM E165/E165M-12, West Conshohocken, USA: American Society for Testing and Materials, 2012.

[53] ASTM, Standard guide for preparation of metallographic specimen, ASTM E3, West Conshohocken, USA: American Society for Testing and Materials, 2017.

[54] Huang, Y., Young, B., "The art of coupon tests," *Journal of Constructional Steel Research,* vol. 96, pp. 159-175, 2014.

[55] Ma, J.L., Chan, T.M., Young, B., "Material properties and residual stresses of cold-formed high strength steel hollow sections," *Journal of Constructional Steel Research,* vol. 109, pp. 152-165, 2015.

[56] Grimault, J.P., Rondal, J., "Comparative study of different measuring methods of residual stresses in steel hollow sections.," CIDECT Report 2L-86/9, International Committee for the Development and Study of Tubular Structures, Geneva, Switzerland, 1986.

[57] Lee, C.K., Chiew, S.P., Jiang, J., "Residual stress study of welded high strength steel thin-walled plate-to-plate joints, part 1: experimental study," *Thin-Walled Structures,* vol. 56, pp. 103-112, 2012.

[58] Lee, C.K., Chiew, S.P., Jiang, J., "Residual stress of high strength steel box T-joints part 1: experimental study," *Journal of Constructional Steel Research,* vol. 93, pp. 20-31, 2014.

[59] ASTM, Standard test method for determining residual stresses by the hole-drilling strain-gauge method, ASTM E837-13a, West Conshohocken, USA: American Society for Testing and Materials, 2013.

Appendix A Measured corner radii and wall thicknesses

The corner radii measurements have been provided in Figure A.1, the corner numbers were marked counter-clock-wisely from the bottom left corner (i.e. Corner 1).

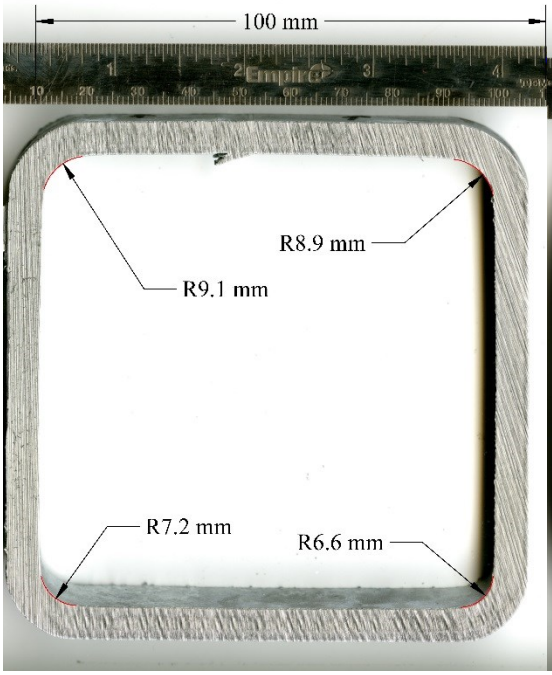

(a) RHS 102×102×6.4

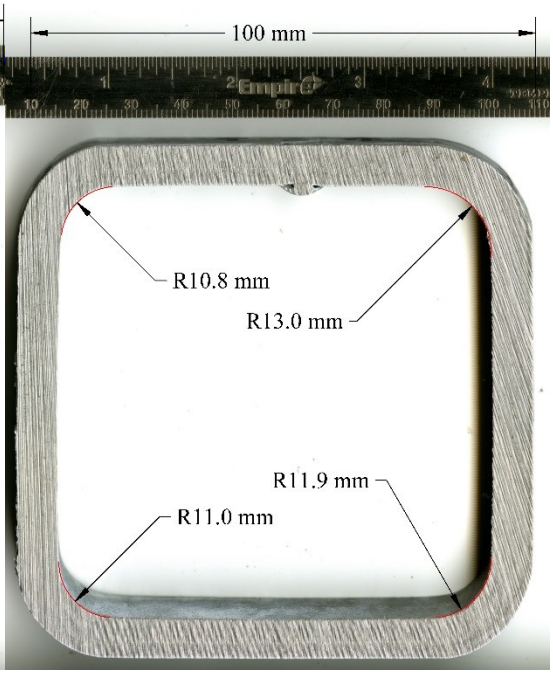

(b) RHS 102×102×7.9

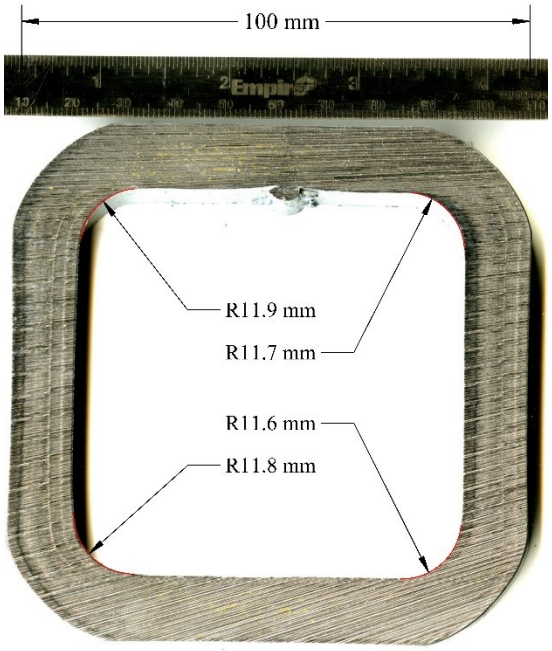

(c) RHS 102×102×13

Figure A.1: Corner radii measurements

16 measurements were taken as illustrated in Figure A.1, the measured results are provided in Table A.1.

Table A.1: Wall thickness measurements

6-C-U							
1	2	3	4	5	6	7	8
6.52	6.40	6.52	6.36	6.25	6.45	6.63	6.37
9	10	11	12	13	14	15	16
6.41	6.31	6.61	6.45	6.22	6.13	6.71	6.20
				Average	6.41	% Diff.	0.14
				Nominal	6.40	Std.	0.16
8-C-U							
1	2	3	4	5	6	7	8
7.83	7.80	7.96	7.80	7.78	7.85	7.92	7.86
9	10	11	12	13	14	15	16
7.89	7.82	7.91	7.80	7.73	7.83	7.73	7.69
				Average	7.83	% Diff.	0.95
				Nominal	7.90	Std.	0.07
13-C-U							
1	2	3	4	5	6	7	8
12.49	12.93	13.07	12.60	12.41	13.03	13.22	12.97
9	10	11	12	13	14	15	16
12.69	12.99	13.35	13.08	12.65	12.75	13.23	13.00
				Average	12.90	% Diff.	0.74
				Nominal	13.00	Std.	0.28

Appendix B Dye Penetrant Inspection images

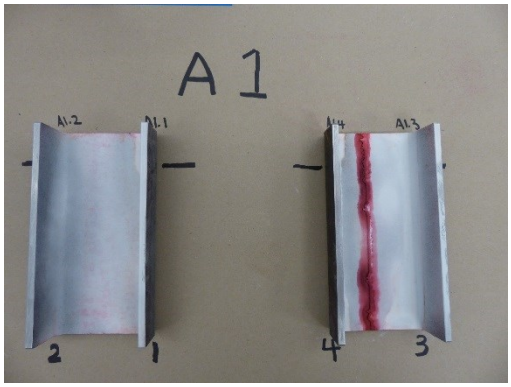

(a) 6-C-U

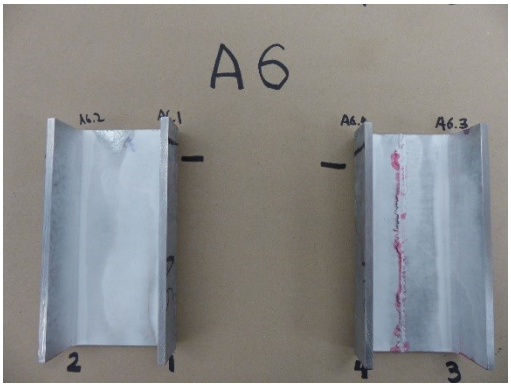

(b) 6-C-G

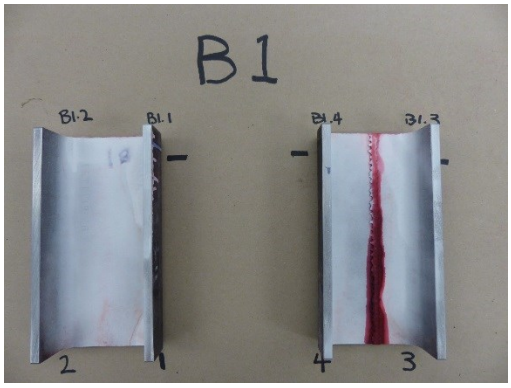

(c) 8-C-U

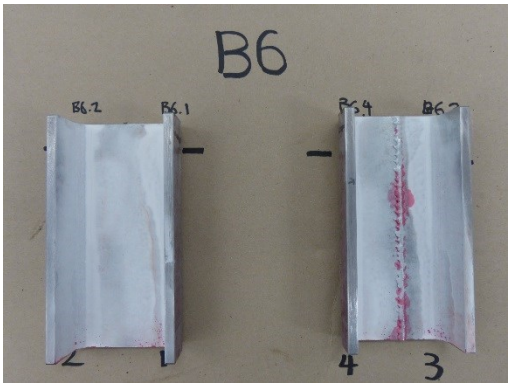

(d) 8-C-G

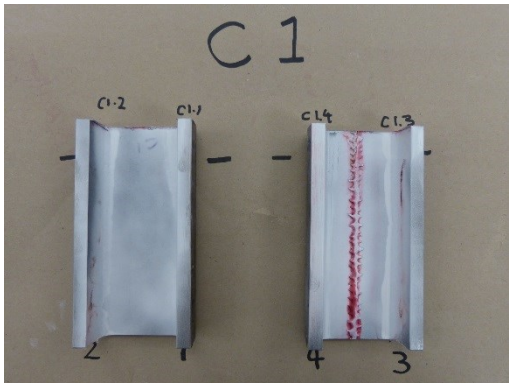

(e) 13-C-U

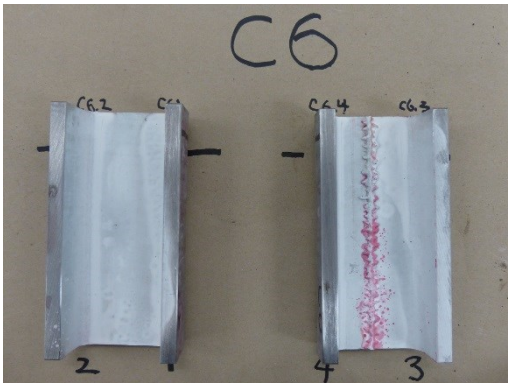

(f) 13-C-G

Figure B.1: Examples of Dye Penetrant Inspections

Appendix C Drawings of tensile coupons

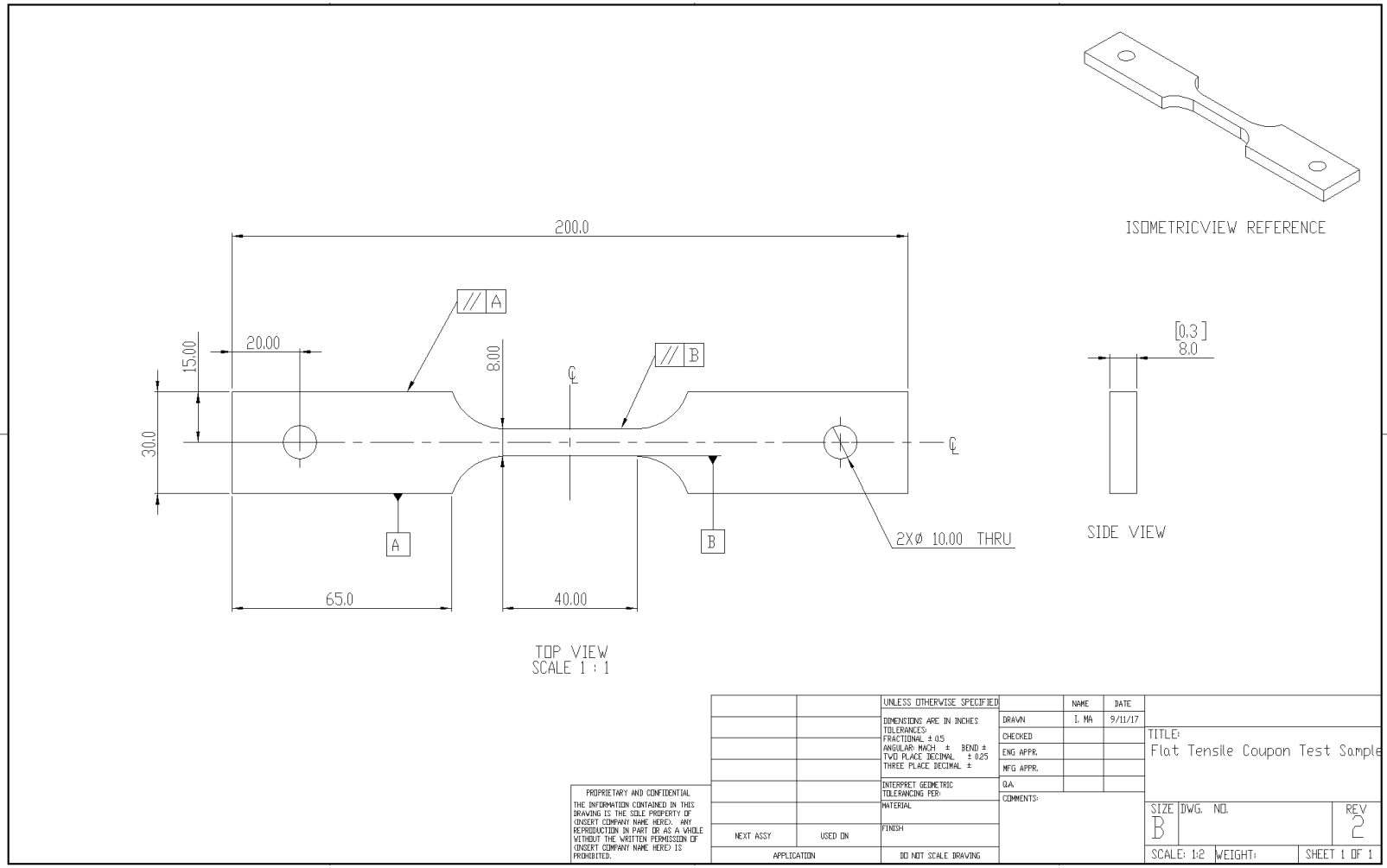

Figure C.1: Sample flat coupon drawing

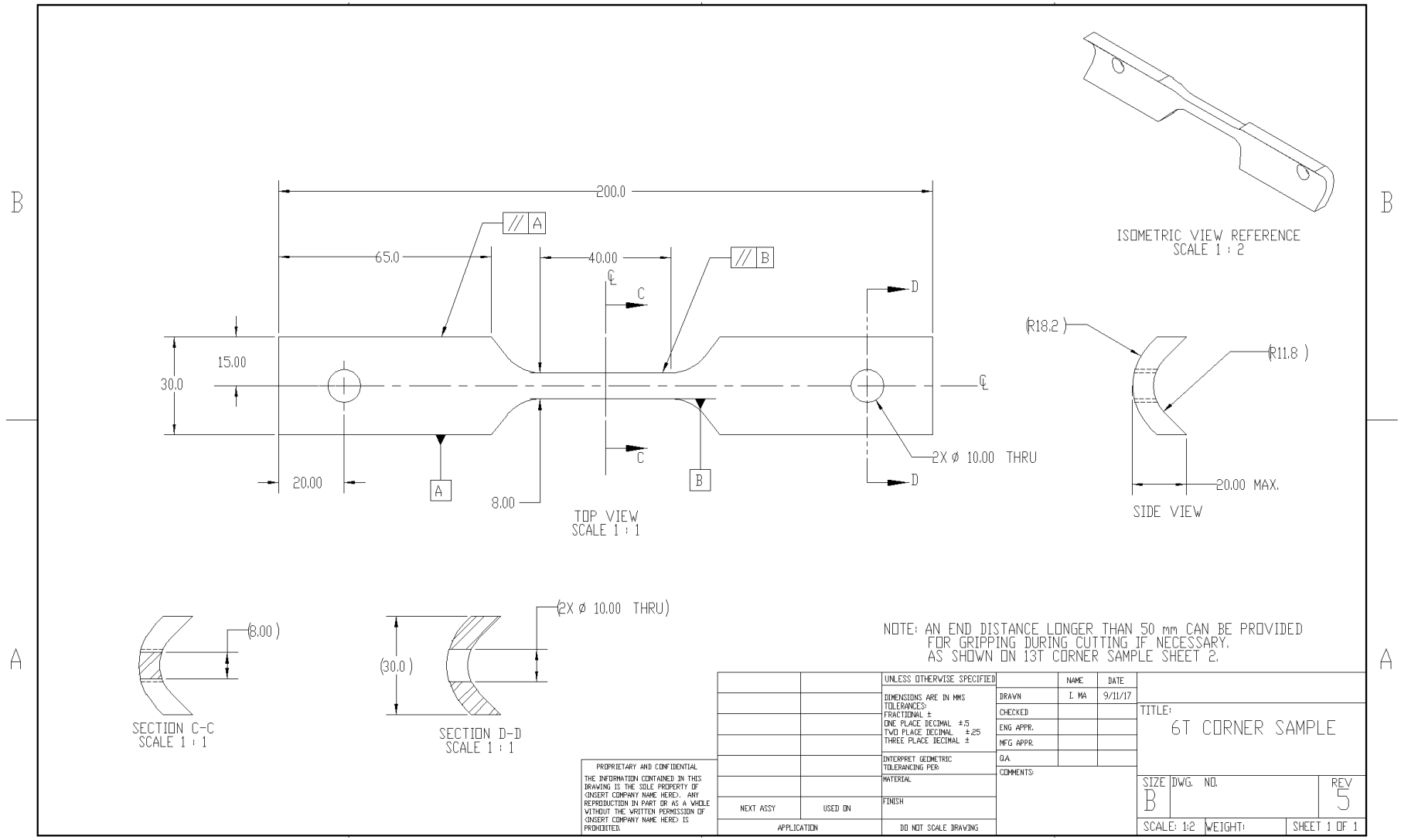

Figure C.2: Sample corner coupon drawing

Appendix D Drawing of special grips

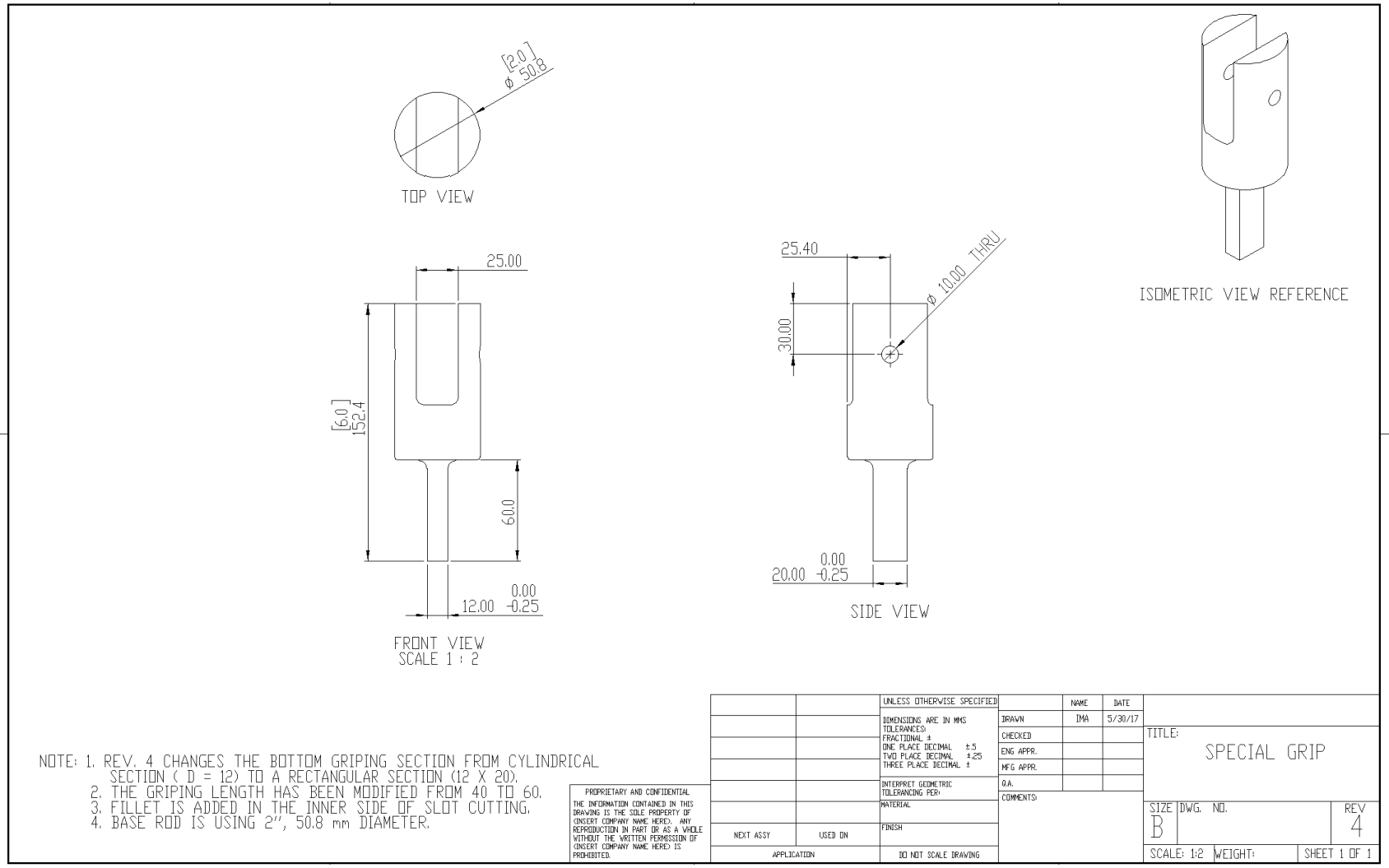

Figure D.1: Drawing of special grip designed for corner coupons

Appendix E Tensile coupon test results

The results of tensile coupon tests for flat coupons are shown in Table E.1 to E.3, and the test results for corner coupons are shown in Table E.4 to E.6. The corner coupons column diagrams including f_y, f_u, f_y/f_u, and ε_{rup} are plotted in Figure E.1 to E12.

Table E.1: Tensile test results, corner coupons, RHS 102×102×6.4

Specimen ID	f_y (MPa)	f_u (MPa)	E (GPa)	ε_{rup} (%)	f_y / f_u
6-C-U-C1	480	524	198	13	0.92
6-450-U-C1	540	602	199	20	0.90
6-595-U-C1	430	496	198	28	0.87
6-C-G-C1	520	560	193	13	0.93
6-450-G-C1	538	591	206	18	0.91
6-595-G-C1	418	496	195	20	0.84
6-C-U-C2	490	540	195	13	0.91
6-450-U-C2	565	626	191	21	0.90
6-595-U-C2	432	505	200	26	0.85
6-C-G-C2	500	544	203	16	0.92
6-450-G-C2	560	613	197	19	0.91
6-595-G-C2	425	487	194	23	0.87
6-C-U-C3	515	559	200	15	0.92
6-450-U-C3	555	610	208	21	0.91
6-595-U-C3	440	507	199	25	0.87
6-C-G-C3	512	553	207	16	0.93
6-450-G-C3	540	594	205	20	0.91
6-595-G-C3	430	491	195	25	0.88
6-C-U-C4	500	551	198	14	0.91
6-450-U-C4	540	603	199	21	0.90
6-595-U-C4	432	500	196	26	0.86
6-C-G-C4	500	557	197	18	0.90
6-450-G-C4	530	586	198	20	0.90
6-595-G-C4	435	495	202	24	0.88

Table E.2: Tensile test results, corner coupons, RHS 102×102×7.9

Specimen ID	f_y (MPa)	f_u (MPa)	E (GPa)	ε_{rup} (%)	f_y / f_u
8-C-U-C1	540	569	199	15	0.95
8-450-U-C1	560	624	208	21	0.90
8-595-U-C1	480	551	200	24	0.87
8-C-G-C1	532	583	206	16	0.91
8-450-G-C1	560	621	197	18	0.90
8-595-G-C1	460	531	201	23	0.87
8-C-U-C2	535	575	197	14	0.93
8-450-U-C2	560	617	195	20	0.91
8-595-U-C2	485	560	207	26	0.87
8-C-G-C2	530	578	207	17	0.92
8-450-G-C2	570	627	194	21	0.91
8-595-G-C2	460	530	201	24	0.87
8-C-U-C3	540	584	204	13	0.92
8-450-U-C3	570	633	206	21	0.90
8-595-U-C3	485	561	197	26	0.86
8-C-G-C3	555	605	199	17	0.92
8-450-G-C3	570	626	207	21	0.91
8-595-G-C3	465	533	205	24	0.87
8-C-U-C4	542	578	204	14	0.94
8-450-U-C4	575	641	210	21	0.90
8-595-U-C4	488	562	205	25	0.87
8-C-G-C4	540	594	191	18	0.91
8-450-G-C4	585	647	203	20	0.90
8-595-G-C4	470	539	200	23	0.87

Table E.3: Tensile test results, corner coupons, RHS 102×102×13

Specimen ID	f_y (MPa)	f_u (MPa)	E (GPa)	ε_{rup} (%)	f_y / f_u
13-C-U-C1	500	551	200	12	0.91
13-450-U-C1	520	582	214	19	0.89
13-595-U-C1	450	537	206	26	0.84
13-C-G-C1	528	586	208	16	0.90
13-450-G-C1	520	577	205	19	0.90
13-595-G-C1	465	549	199	25	0.85
13-C-U-C2	520	581	197	14	0.89
13-450-U-C2	525	594	194	19	0.88
13-595-U-C2	470	555	207	26	0.85
13-C-G-C2	540	595	201	18	0.91
13-450-G-C2	502	564	204	19	0.89
13-595-G-C2	470	549	207	25	0.86
13-C-U-C3	503	555	198	15	0.91
13-450-U-C3	528	587	198	20	0.90
13-595-U-C3	457	544	204	25	0.84
13-C-G-C3	532	590	209	19	0.90
13-450-G-C3	520	585	209	20	0.89
13-595-G-C3	458	545	201	25	0.84
13-C-U-C4	500	563	197	15	0.89
13-450-U-C4	540	605	198	18	0.89
13-595-U-C4	460	549	200	26	0.84
13-C-G-C4	550	611	208	16	0.90
13-450-G-C4	520	582	200	18	0.89
13-595-G-C4	465	553	205	25	0.84

Table E.4: Tensile test results, flat coupons, RHS 102×102×6.4

Specimen ID	f_y (MPa)	f_u (MPa)	E (GPa)	ε_{rup} (%)	f_y / f_u	$f_{yf,avg}$ (MPa)	$f_{uf,avg}$ (MPa)	E_{avg} (GPa)	$\varepsilon_{rup,avg}$ (%)	$f_{yf,avg} / f_{uf,avg}$
6-C-U-F1	410	481	201	29	0.85	415	482	199	30	0.86
6-C-U-F2	420	483	197	30	0.87					
6-450-U-F1	423	502	206	31	0.84	427	505	202	31	0.85
6-450-U-F2	430	507	197	30	0.85					
6-595-U-F1	388	486	206	33	0.80	384	486	200	33	0.79
6-595-U-F2	380	486	194	33	0.78					
6-C-G-F1	440	504	207	27	0.87	445	509	203	27	0.88
6-C-G-F2	450	513	198	26	0.88					
6-450-G-F1	425	501	200	31	0.85	430	502	203	31	0.86
6-450-G-F2	435	502	206	30	0.87					
6-595-G-F1	368	448	203	33	0.82	369	447	203	32	0.83
6-595-G-F2	370	446	202	30	0.83					

Table E.5: Tensile test results, flat coupons, RHS 102×102×7.9

Specimen ID	f_y (MPa)	f_u (MPa)	E (GPa)	ε_{rup} (%)	f_y / f_u	$f_{yf,avg}$ (MPa)	$f_{uf,avg}$ (MPa)	E_{avg} (GPa)	$\varepsilon_{rup,avg}$ (%)	$f_{yf,avg} / f_{uf,avg}$
8-C-U-F1	450	506	198	25	0.89	458	509	198	25	0.90
8-C-U-F2	465	512	197	24	0.91					
8-450-U-F1	463	531	206	25	0.87	468	539	208	26	0.87
8-450-U-F2	473	547	210	26	0.87					
8-595-U-F1	410	504	205	32	0.81	409	505	206	31	0.81
8-595-U-F2	408	506	207	30	0.81					
8-C-G-F1	480	524	194	23	0.92	478	530	194	22	0.91
8-C-G-F2	475	535	193	21	0.89					
8-450-G-F1	463	531	204	23	0.87	469	538	202	24	0.87
8-450-G-F2	475	545	199	24	0.87					
8-595-G-F1	410	497	194	30	0.82	413	501	202	29	0.82
8-595-G-F2	415	505	209	28	0.82					

Table E.6: Tensile test results, flat coupons, RHS 102×102×13

Specimen ID	f_y (MPa)	f_u (MPa)	E (GPa)	ε_{rup} (%)	f_y / f_u	$f_{yf,avg}$ (MPa)	$f_{uf,avg}$ (MPa)	E_{avg} (GPa)	$\varepsilon_{rup,avg}$ (%)	$f_{yf,avg} / f_{uf,avg}$
13-C-U-F1	470	541	202	23	0.87	483	549	201	22	0.88
13-C-U-F2	495	557	200	21	0.89					
13-450-U-F1	480	593	206	25	0.86	480	566	201	25	0.88
13-450-U-F2	480	538	196	24	0.89					
13-595-U-F1	442	535	201	28	0.83	433	527	196	30	0.83
13-595-U-F2	423	518	191	32	0.82					
13-C-G-F1	478	542	208	21	0.88	493	555	207	21	0.89
13-C-G-F2	508	568	206	20	0.90					
13-450-G-F1	510	590	207	24	0.87	485	559	202	25	0.87
13-450-G-F2	460	527	197	25	0.87					
13-595-G-F1	458	542	204	28	0.84	439	527	200	30	0.83
13-595-G-F2	420	512	196	31	0.82					

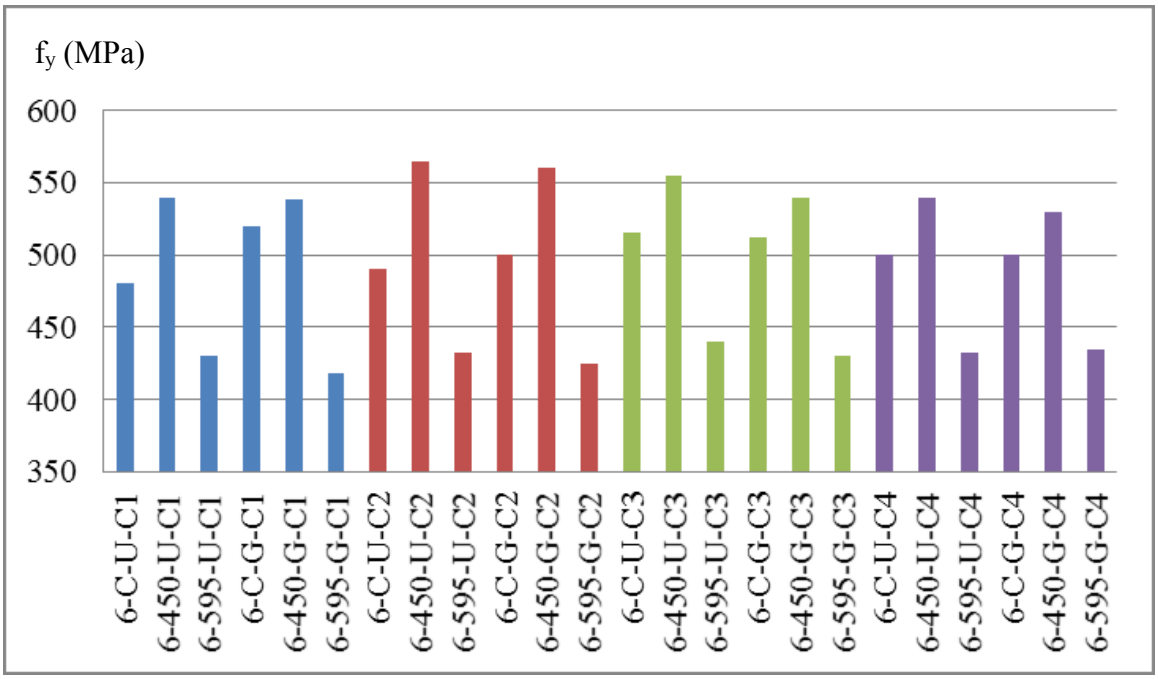

Figure E.1: Corner coupons, RHS 102×102×6.4, f_y diagram

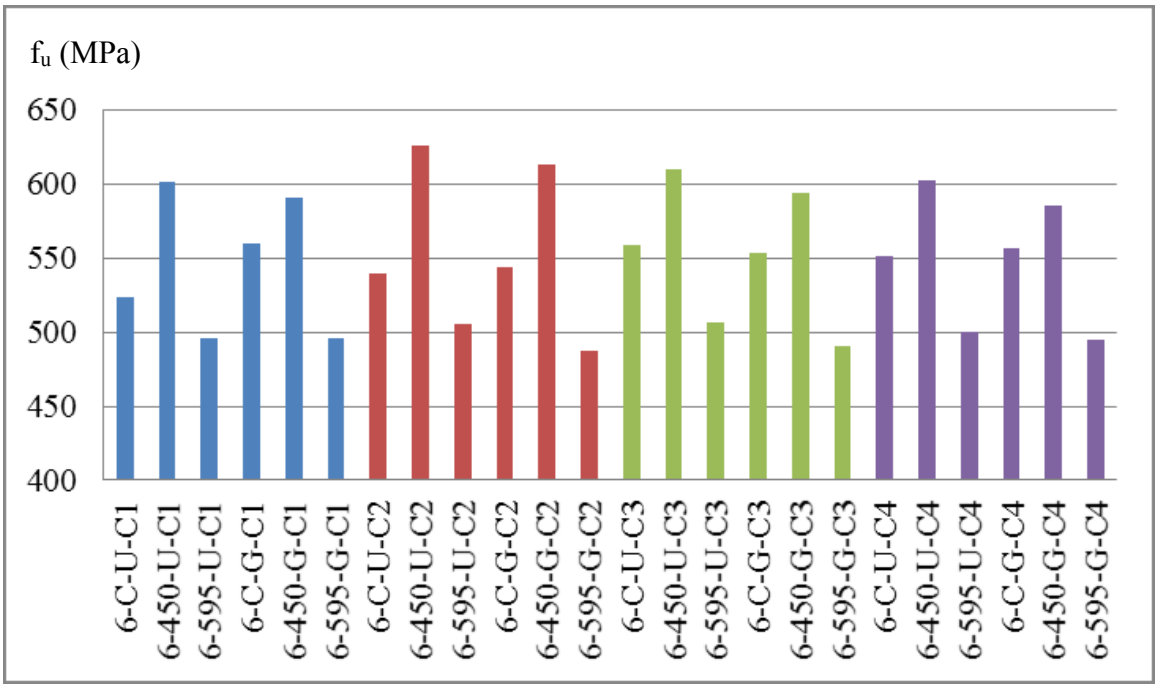

Figure E.2: Corner coupons, RHS 102×102×6.4, f_u diagram

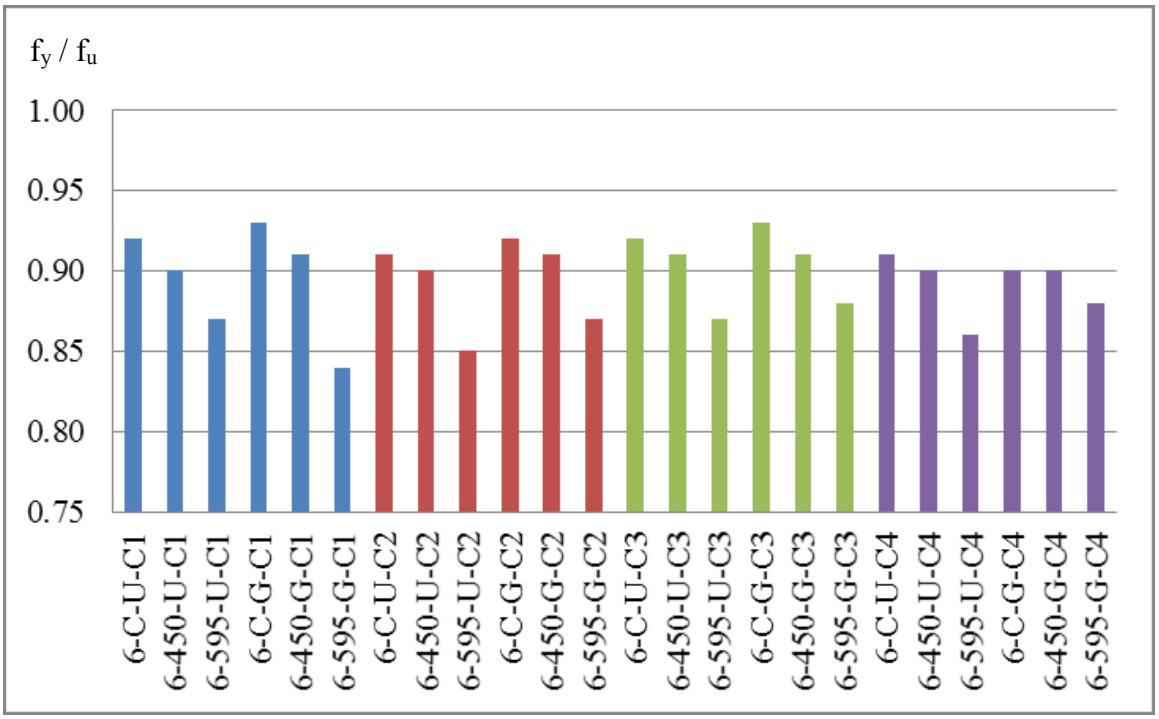

Figure E.3: Corner coupons, RHS 102×102×6.4, f_y/f_u diagram

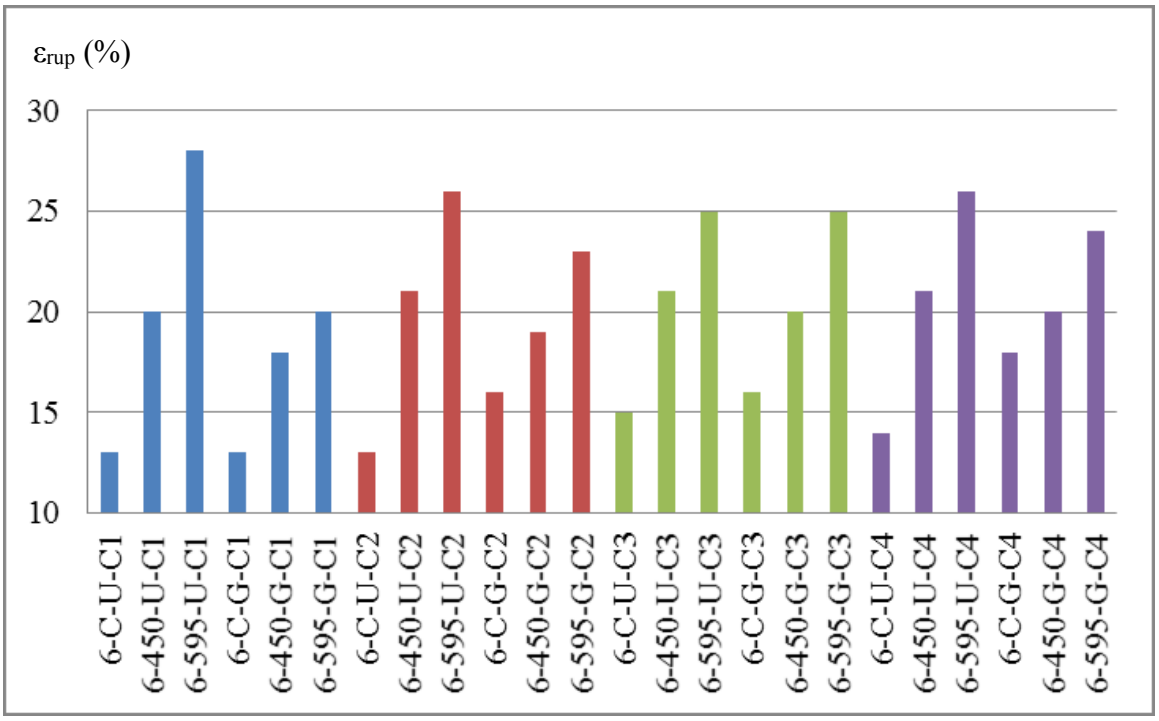

Figure E.4: Corner coupons, RHS 102×102×6.4, ε_{rup} diagram

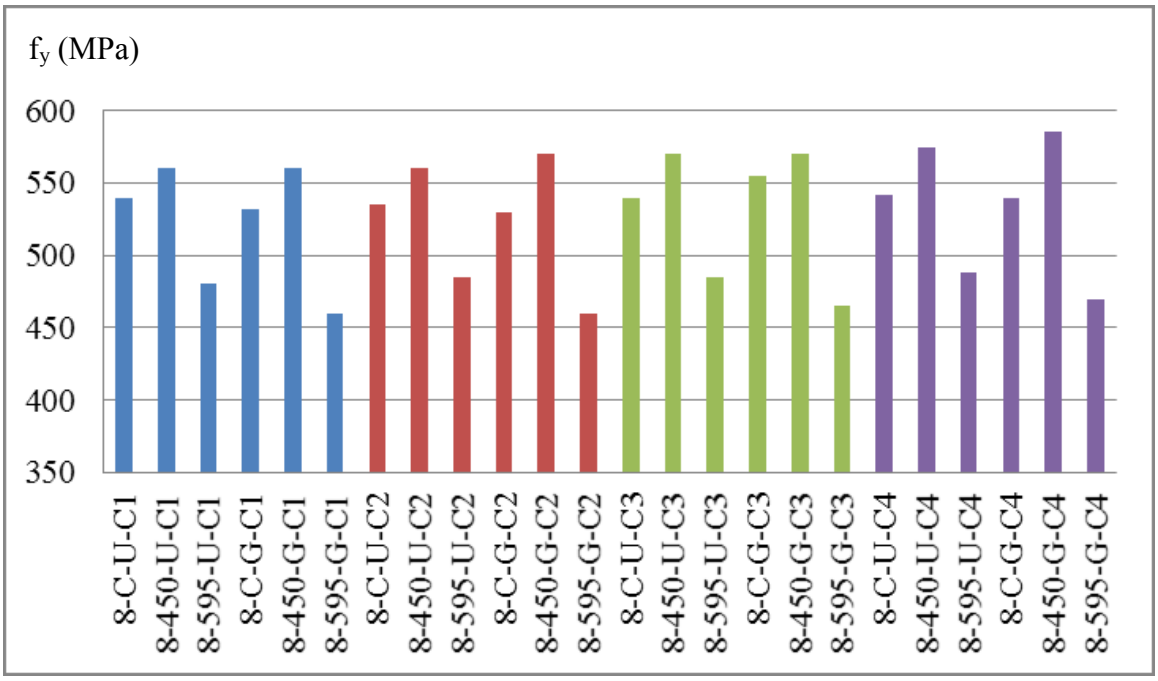

Figure E.5: Corner coupons, RHS 102×102×7.9, f_y diagram

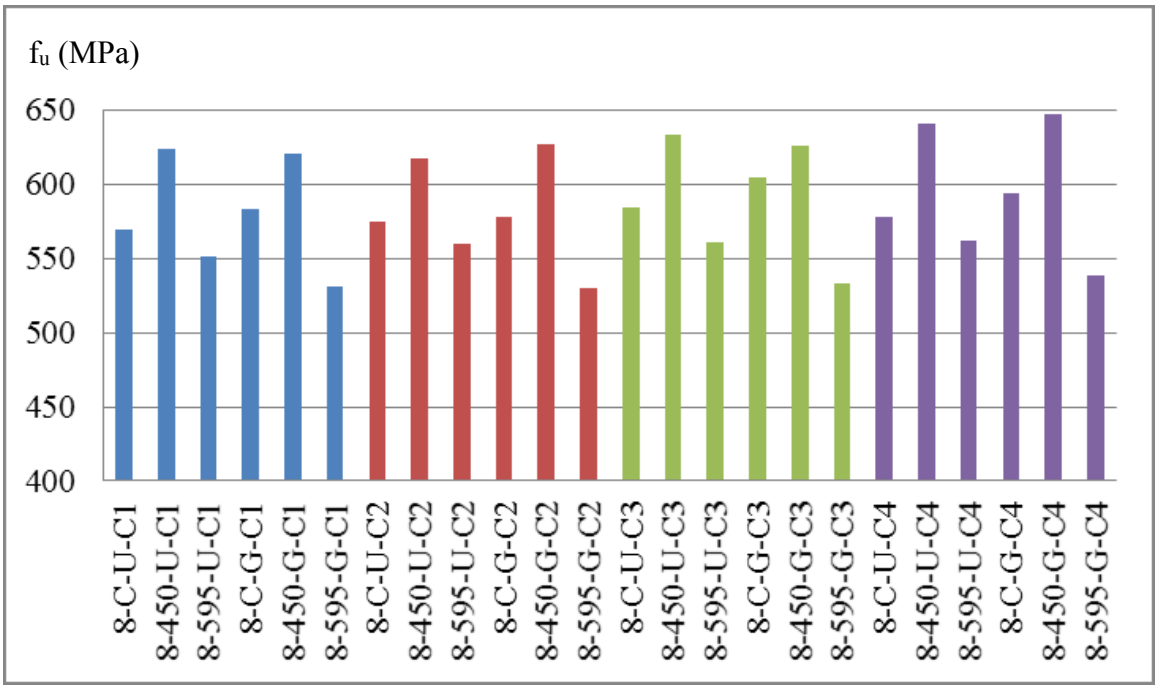

Figure E.6: Corner coupons, RHS 102×102×7.9, f_u diagram

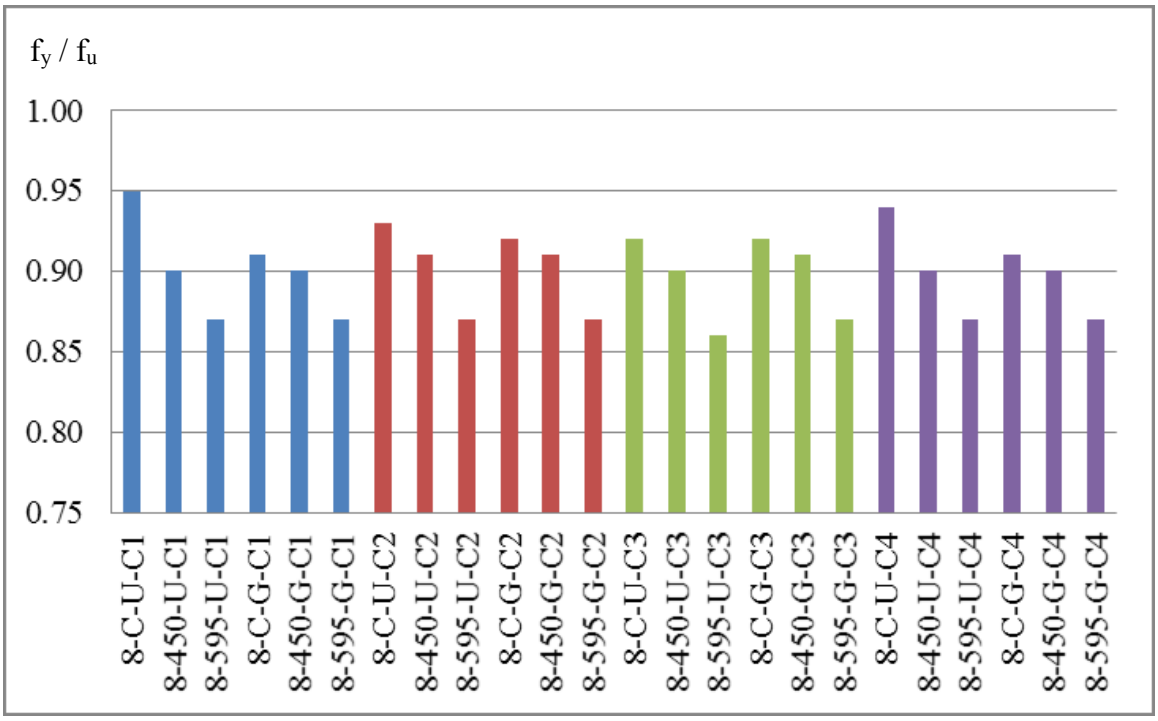

Figure E.7: Corner coupons, RHS 102×102×7.9, f_y/f_u diagram

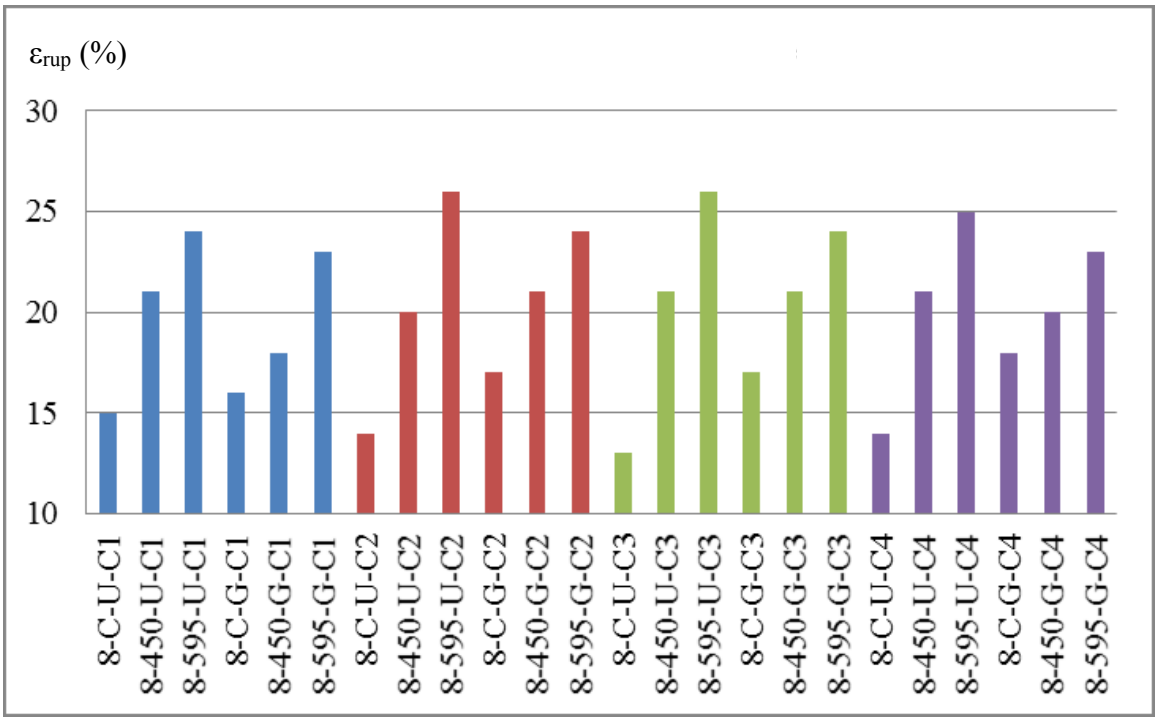

Figure E.8: Corner coupons, RHS 102×102×7.9, ε_{rup} diagram

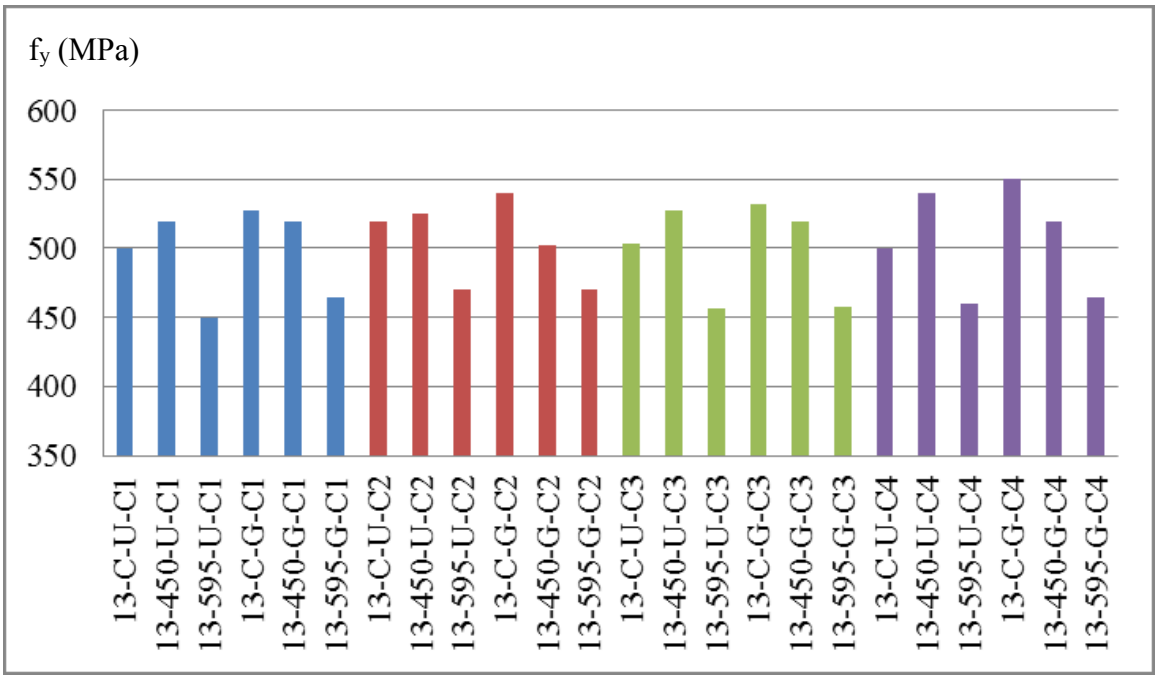

Figure E.9: Corner coupons, RHS 102×102×13, f_y diagram

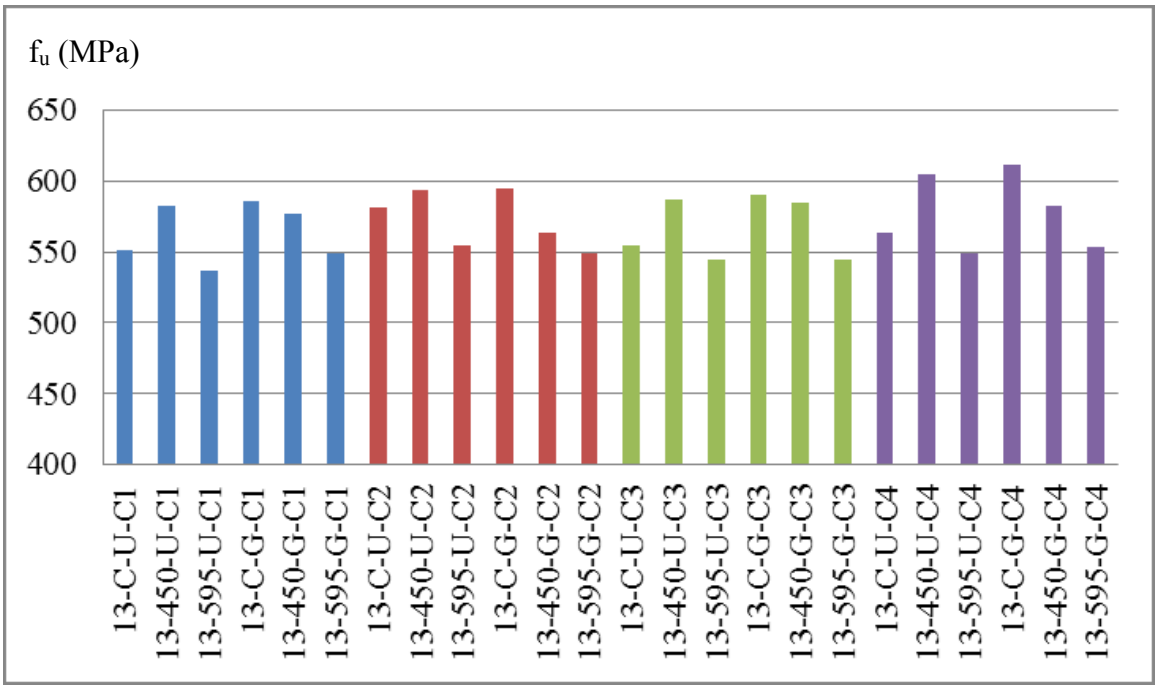

Figure E.10: Corner coupons, RHS 102×102×13, f_u diagram

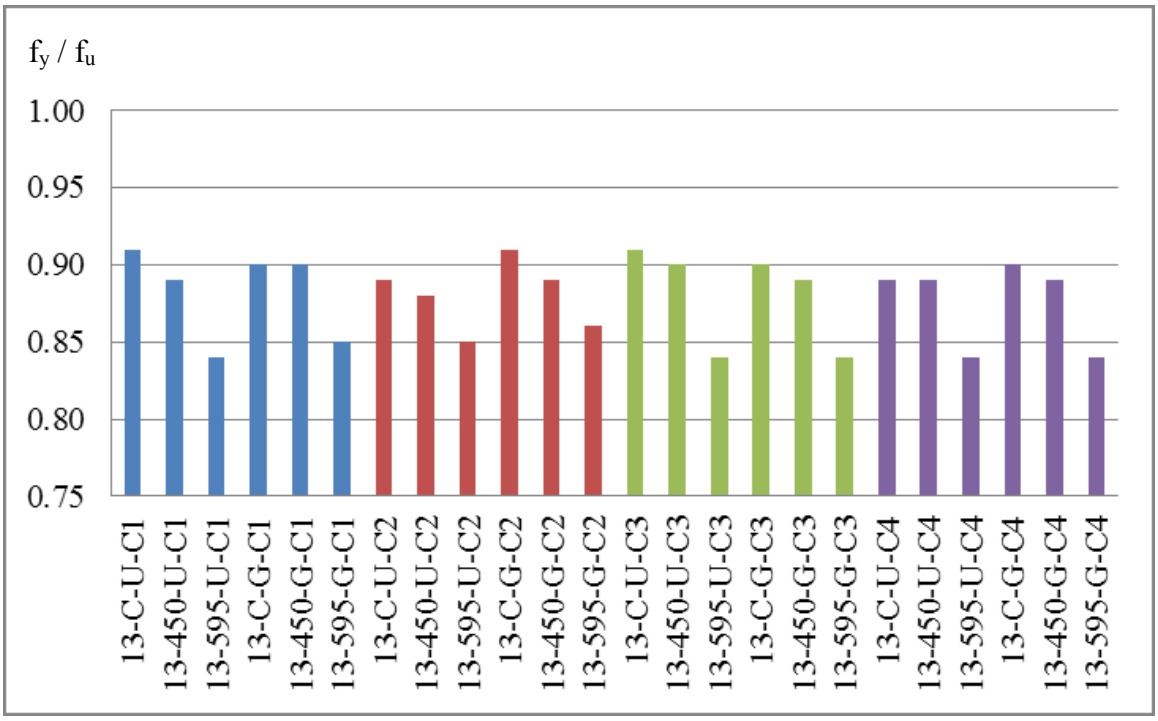

Figure E.11: Corner coupons, RHS 102×102×13, f_y/f_u diagram

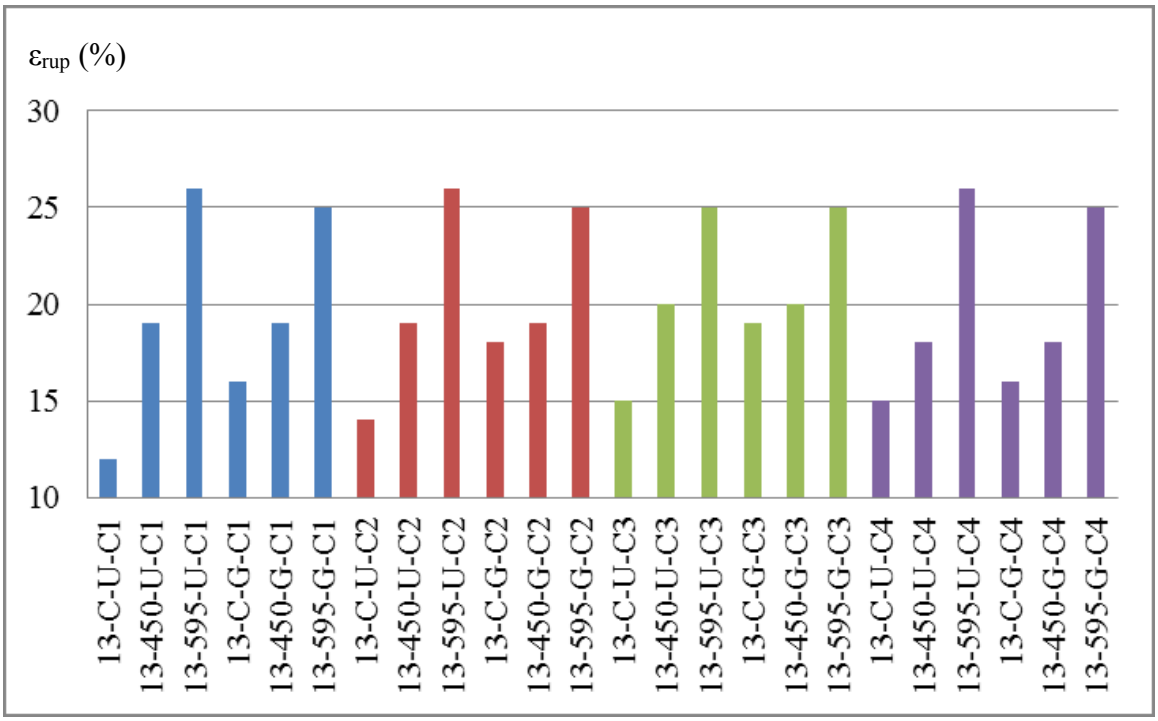

Figure E.12: Corner coupons, RHS 102×102×13, ε_{rup} diagram

Appendix F Residual stress results

The results of residual stress using hole-drill method have been shown in this section. Table F.1 shows the measured stresses in longitudinal and transverse directions, and the maximum and minimum principle stresses on the free end. Table F.2 presents the middle sections results. The relevant column diagrams have been plotted in Figure F.1 and F.2 respectively.

Table F.1: Measurements of residual stresses (free end)

Specimen ID	$\sigma_{rs,long}$	$\sigma_{rs,tran}$	σ_{max}	σ_{min}
6-C-U C1	181	106	228	59
6-450-U C1	117	87	140	64
6-595-U C1	68	67	88	47
6-C-U C2	217	154	289	82
6-450-U C2	167	128	260	35
6-595-U C2	71	65	89	47
6-C-U C3	168	145	201	112
6-450-U C3	115	96	177	34
6-595-U C3	61	59	82	38
6-C-U C4	153	97	225	25
6-450-U C4	101	77	103	75
6-595-U C4	66	59	82	43
8-C-U C1	244	145	264	125
8-C-G C1	155	121	157	119
8-450-U C1	127	107	131	103
8-595-U C4	80	66	110	35
8-C-U C2	211	110	243	78
8-C-G C2	131	98	172	56
8-450-U C2	118	82	153	48
8-595-U C2	70	41	87	24
8-C-U C3	158	90	194	54
8-450-U C3	88	70	98	61
8-595-U C3	54	40	80	14
8-C-U C4	249	141	293	96
8-450-U C4	166	103	166	102
8-595-U C4	80	66	110	35
13-C-U C1	211	141	274	78
13-C-G C1	127	91	138	79
13-450-U C1	121	70	148	42
13-595-U C1	67	53	73	43
13-C-U C2	244	187	269	163
13-C-G C2	133	110	175	67
13-450-U C2	136	91	178	49
13-595-U C2	68	59	76	51
13-C-U C3	172	141	249	64
13-450-U C3	123	109	142	90
13-595-U C3	56	45	73	28
13-C-U C4	159	111	220	50
13-450-U C4	113	82	130	66
13-595-U C4	51	39	59	31

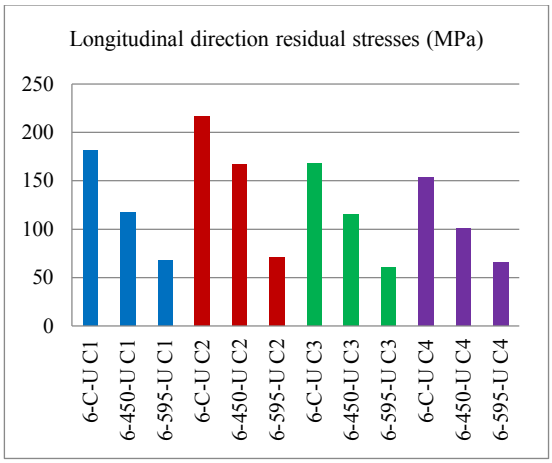

(a) Longitudinal, RHS 102×102×6.4

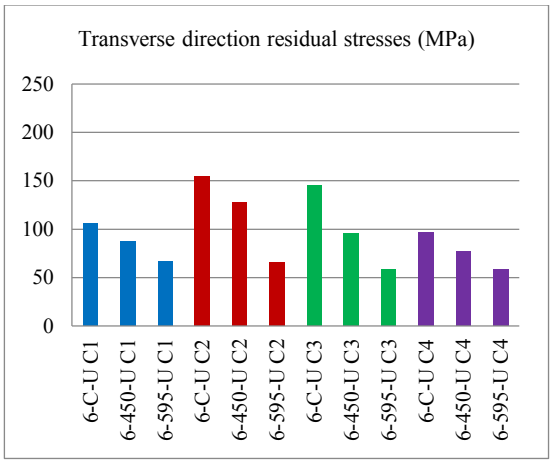

(b) Transverse, RHS 102×102×6.4

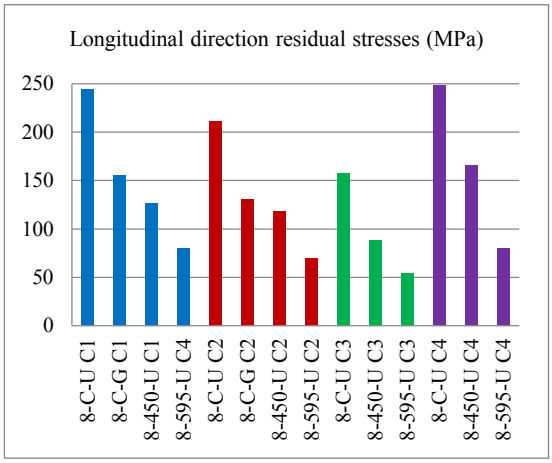

(c) Longitudinal, RHS 102×102×7.9

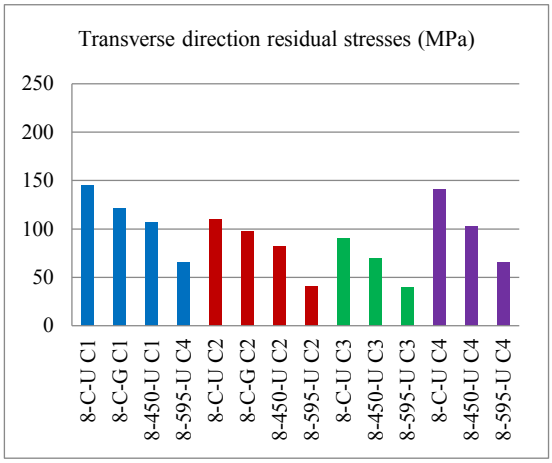

(d) Transverse, 102×102×7.9

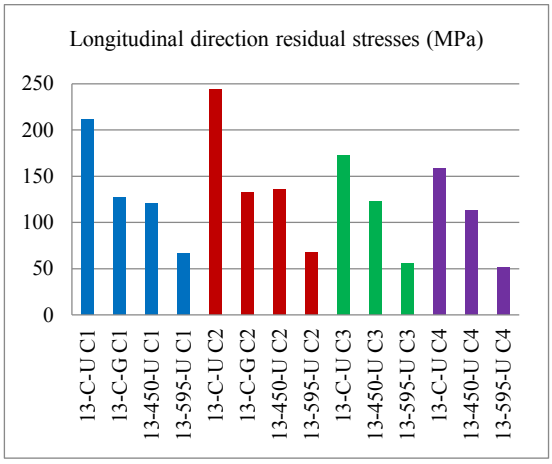

(e) Longitudinal, RHS 102×102×13

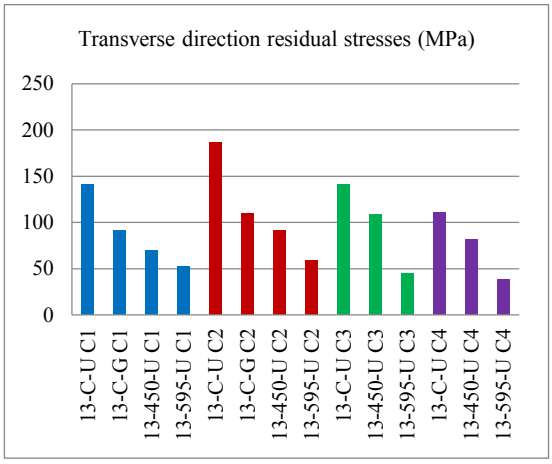

(f) Transverse, RHS 102×102×13

Figure F.1: Measurements of residual stresses (free end)

Table F.2: Measurements of residual stresses (middle section)

Specimen ID	$\sigma_{rs,long}$	$\sigma_{rs,tran}$	σ_{max}	σ_{min}
8-C-U C1 M	448	318	448	318
8-C-G C1 M	243	192	303	132
8-C-U C2 M	420	265	425	261
8-C-G C2 M	232	145	233	144
13-C-U C1 M	376	184	379	180
13-C-G C1 M	182	126	234	74
13-C-U C2 M	448	232	456	225
13-C-G C2 M	167	130	228	68

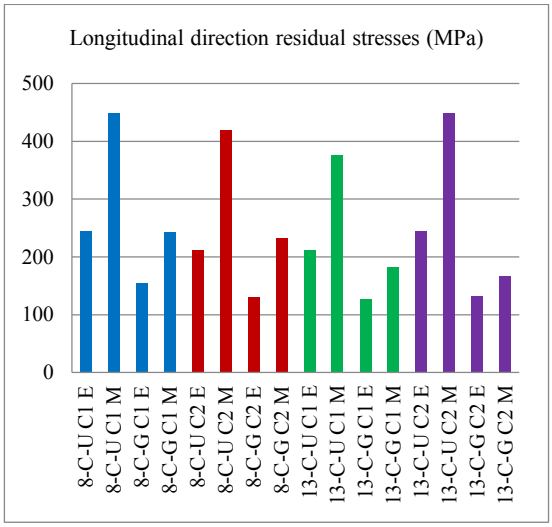

(a) Longitudinal direction

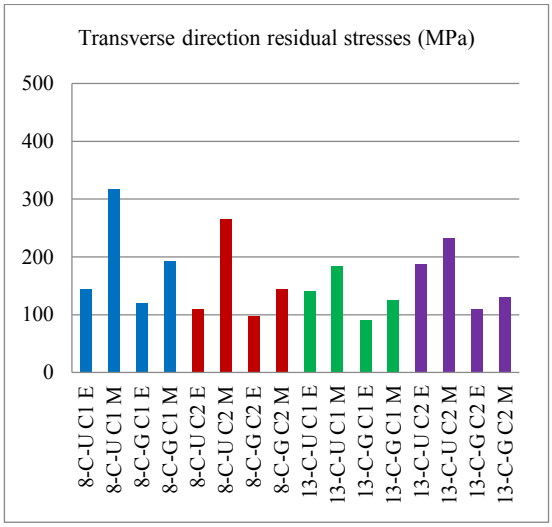

(b) Transverse direction

Figure F.2: Comparison of free end and middle section